REPORT No. 648

DESIGN CHARTS FOR PREDICTING DOWNWASH ANGLES AND WAKE CHARACTERISTICS BEHIND PLAIN AND FLAPPED WINGS

By ABE SILVERSTEIN and S. KATZOFF

SUMMARY

Equations and design charts are given for predicting the downwash angles and the wake characteristics for power-off conditions behind plain and flapped wings of the types used in modern design practice. The downwash charts cover the cases of elliptical wings and wings of taper ratios 1, 2, 3, and 5, with aspect ratios of 6, 9, and 12, having flaps covering 0, 40, 70, and 100 percent of the span. Curves of the span load distributions for all these cases are included. Data on the lift and the drag of flapped airfoil sections and curves for finding the contribution of the flap to the total wing lift for different types of flap and for the entire range of flap spans are also included. The wake width and the distribution of dynamic pressure across the wake are given in terms of the profile-drag coefficient and the distance behind the wing. A method of estimating the wake position is also given.

The equations and the charts are based on theory that has been shown in a previous report to be in agreement with experiment.

INTRODUCTION

In a recent paper (reference 1) methods are developed for predicting downwash angles and wake characteristics for power-off conditions behind airfoils of known span loading. The calculation of downwash involves several simplifying assumptions that are shown to be justified. Wake characteristics are given by empirical expressions derived from experimental data and are in agreement with available theory.

In order to make the methods of reference 1 readily applicable for design purposes, charts have been prepared covering the range of modern design practice. These charts are given in the present paper. Included are curves of the lift and the drag of flapped airfoil sections and charts for finding the contributions of the different types of flap to the total wing lift. Information is also presented for determining the position of the wake, its width, and the distribution of dynamic pressure across it.

The downwash charts are for elliptical wings and for wings of taper ratios 1, 2, 3, and 5, with aspect ratios of 6, 9, and 12, having flaps covering 0, 40, 70, and 100 percent of the span. The explanatory text accompanying the charts is sufficiently complete to permit their use without study of reference 1.

SYMBOLS

C_L, lift coefficient.
C_{L_w}, lift coefficient at a particular angle of attack, flaps up.
C_{L_f}, increase of lift coefficient, at the same angle of attack, upon deflecting the flap.
c_l, section lift coefficient.
Δc_l, increment of section lift coefficient corresponding to a flap deflection (two-dimensional).
c_{d_0}, section profile-drag coefficient.
c, wing chord.
c_f, flap chord.
b, wing span.
b_f, flap span.
S, wing area.
x, longitudinal distance from quarter-chord point.
y, lateral distance from symmetry plane.
z, vertical distance from quarter-chord point.
s, vortex semispan, in wing semispans.
Γ, vortex strength.
w, induced vertical velocity.
g, downwash factor.
ϵ, downwash angle.
h, downward displacement, measured normal to the relative wind, of the center line of the wake and the trailing vortex sheet from its origin at the trailing edge.
m, vertical distance of the elevator hinge axis from the wake origin, measured perpendicular to the relative wind.
ξ, distance behind the trailing edge.
ζ, wake half-width.
ζ', vertical distance from wake center line.
η, loss in dynamic pressure at wake center, fraction of free-stream dynamic pressure q.
η', loss in dynamic pressure, fraction of free-stream dynamic pressure q.
k, correction for locating wake origin.
δ_f, flap angle.

RÉSUMÉ OF THEORY

Downwash, plain wings.—The downwash behind a wing is mainly a function of the wing loading and is a manifestation of the associated vortex system. This vortex system comprises the bound, or lifting, vortex considered localized at the quarter-chord line and the vortex sheet that is shed from the trailing edge. If the strength of the bound vortex at distance s from the airfoil center is Γ, the vorticity per unit spanwise length in the sheet as it leaves the trailing edge is $-d\Gamma/ds$.

A first approximation to the downwash is obtained by assuming the sheet to originate at the quarter-chord line and to extend unchanged indefinitely downstream, the vortex system thereby consisting of elementary U-vortices (or horseshoe vortices) of semispan s and strength $-(d\Gamma/ds)ds$ to which the Biot-Savart equation is applicable. The actual sheet, however, does not extend unaltered from the lifting line to infinity because, as a result of the air motions that the vortex system itself creates, it is rapidly displaced downward and deformed.

For purposes of calculation of the downwash angle at the tail, a satisfactory second approximation is obtained by neglecting the deformation and considering the entire sheet to be uniformly displaced downward by an amount equal to the displacement of the center of the sheet near the tail. This displacement, furthermore, can be readily calculated since the sheet follows the downflow which, with reasonable accuracy, may be taken as that given by the first approximation. Inasmuch as the downwash depends to a predominant extent on the trailing vortex sheet, a vertical displacement of the sheet causes a vertical displacement of the entire downwash pattern by the same amount.

The strength of the vortex system is proportional to C_L; hence, the downwash angle ϵ and the displacement h must also be proportional to C_L. At higher lifts, however, there are three disturbing effects, all of which tend to increase the downwash above the sheet and to decrease it below. These factors are: (1) The effect of the strong tip vortices that, owing to the curvature of the sheet, are above the center; (2) the effect of the bound vortex that, owing to the downward displacement of the sheet relative to it, similarly contributes more to the downwash above than below it; and (3) the flow of air into the wake, which is coincident with the trailing vortex sheet.

Downwash, flapped wings.—The effect of a flap on the downwash depends upon its effect on the span load distribution. The change in loading upon lowering a given flap is nearly independent of the angle of attack, and the absolute change in the lift coefficient at any section c_l is approximately proportional to the total increase in the wing lift coefficient C_{L_f}. The resultant loading and vortex systems being the sums of those of the plain wing and of the flap, the resultant downwash is the sum of that due to the plain wing at the given attitude and that due to the flap. The component due to the flap is proportional to C_{L_f}. The vortex-sheet origin lies between the trailing edges of the plain wing and of the flap. Its vertical displacement is, like the downwash, the sum of that due to the plain wing and that due to the flap.

For wings with flaps, increased importance attaches to the three disturbing effects mentioned for plain wings. The wake, in particular, requires consideration where high-drag flaps are used.

The wake.—The wake is characterized by a loss in total pressure, the deficiency being a maximum at its center and decreasing to zero at a fairly well-defined wake edge. Its center line coincides with that of the trailing vortex sheet. On account of turbulent mixing with the surrounding air, the maximum total-pressure loss decreases with distance downstream, whereas the width of the wake increases. The integrated loss in total pressure across the wake remains nearly constant and is proportional to the profile drag of the wing section from which the wake was shed.

DOWNWASH CHARTS

Plan forms.—The downwash charts of figures 1 to 15 contain four groups of diagrams. In the first column of each chart are shown the plan forms of the wings for which the computations were made. Consistent with the assumption made in the calculations that there is no sweepback of the lifting line, the quarter-chord line is drawn perpendicular to the center line in every case. The tips are shown rounded for a spanwise distance equal to the tip chord, as was done in reference 2. Although the flap chord is shown as 20 percent of the wing chord, the actual value of c_f/c is immaterial as long as it is constant over the entire span of the flap. In actual practice, this condition is not always maintained. As long as the variation of c_f/c remains within the usual limits, however, this source of error is of secondary importance.

Span load distributions.—The span load distributions are shown in the second column of each figure. The distribution for the plain wing was obtained from reference 2. The distributions for the flap conditions were computed by the Lotz method (reference 3). In the computations, the Fourier coefficients for the chord distribution were found by Pearson's system (reference 4) and the Fourier coefficients for the angle distribution were found by the usual method of integration. Ten terms of the series for the loading were derived, which are adequate to give the shape of the loading curve except near the flap tip, where a reasonable number of terms does not suffice to give the shape accurately. The curves are therefore more or less arbitrarily drawn in this region, the main condition being that the slope be infinite at the position of the flap tip.

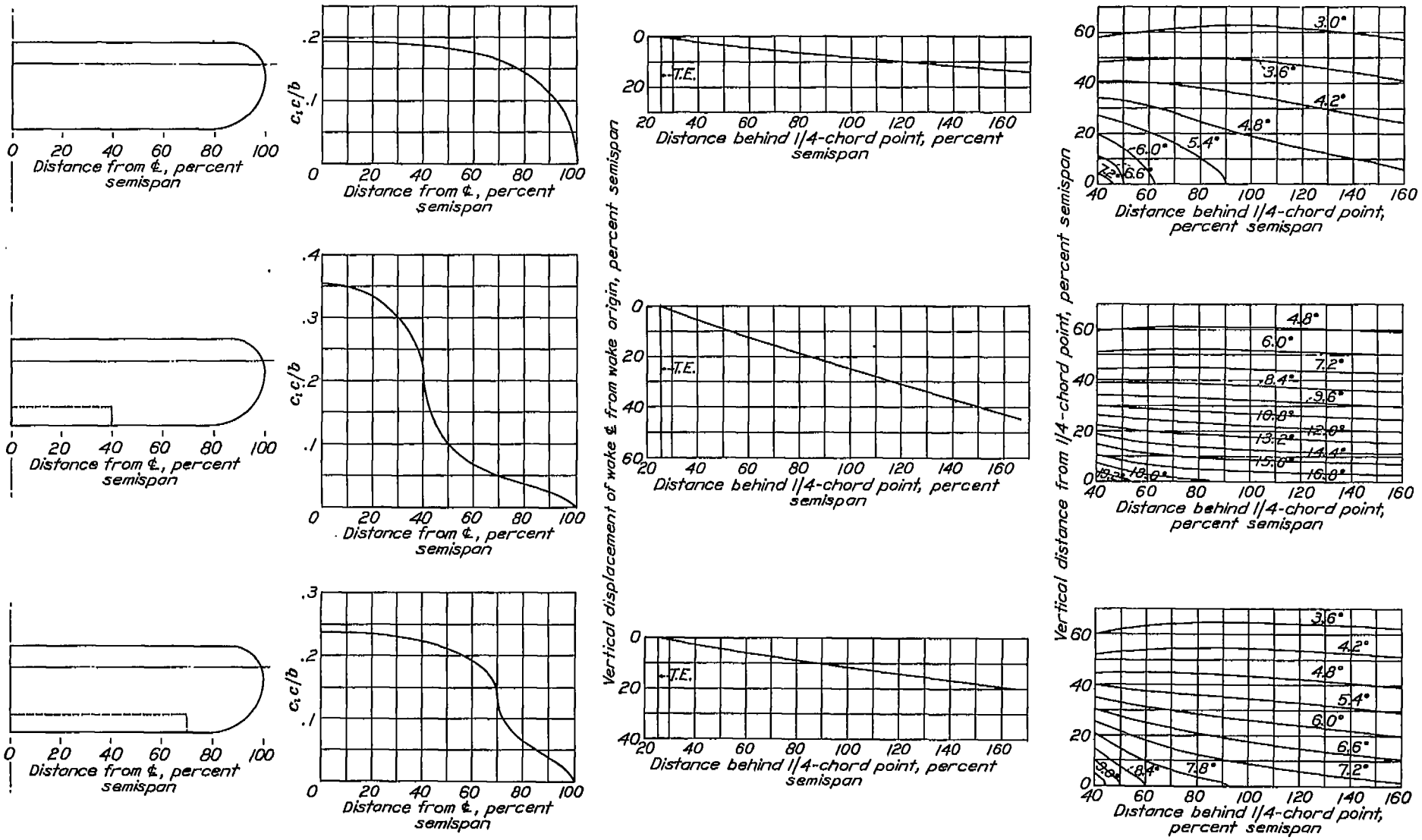

FIGURE 1.—Design charts showing load distribution, downwash displacement, and downwash angles. Plain wing, 0.4b and 0.7b flaps; C_L and C_{l_f}, 1.0; taper, 1:1; aspect ratio, 6.

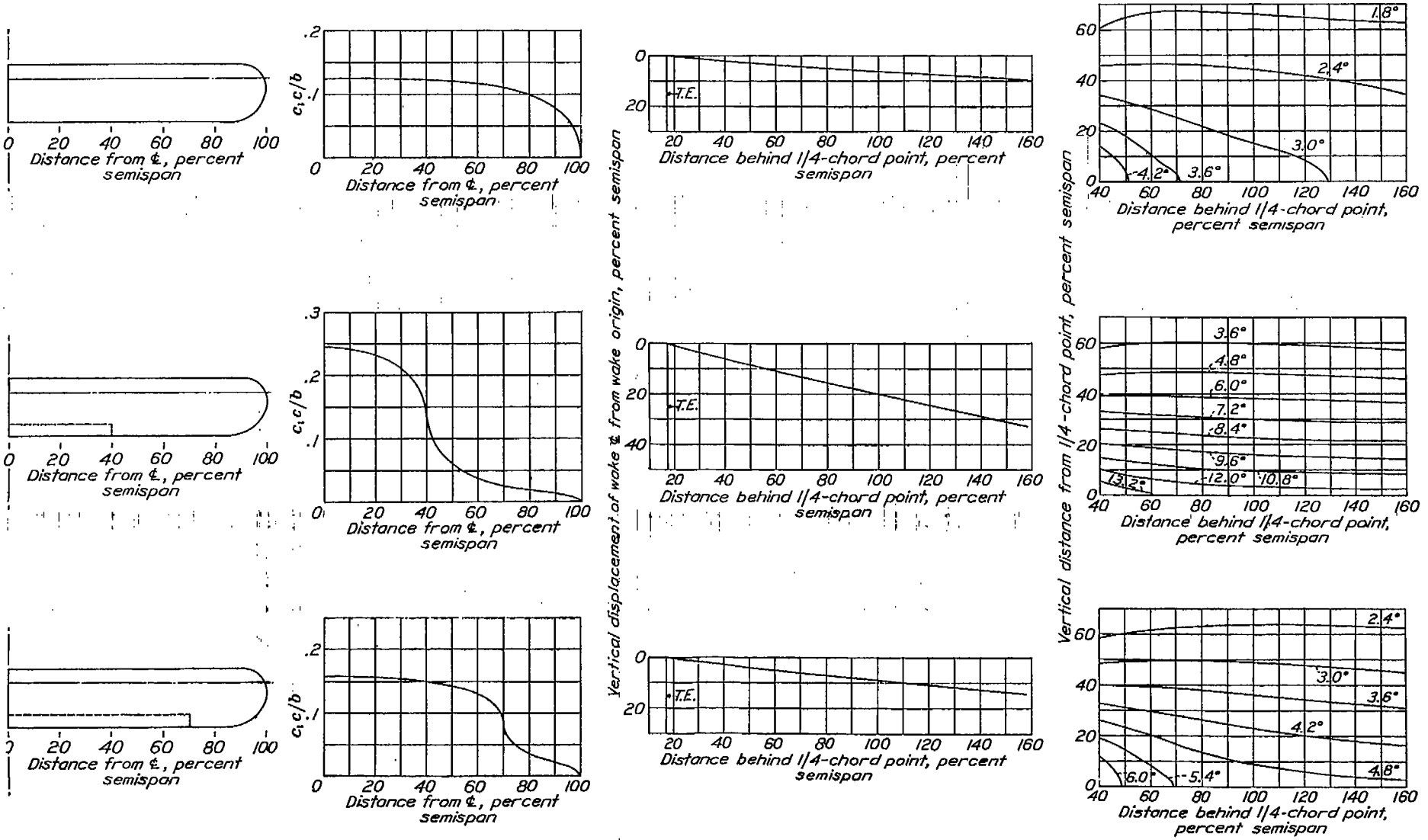

FIGURE 2.—Design charts showing load distribution, downwash displacement, and downwash angles. Plain wing, 0.4b and 0.7b flaps; C_L and C_{l_p} 1.0; taper, 1:1; aspect ratio, 9.

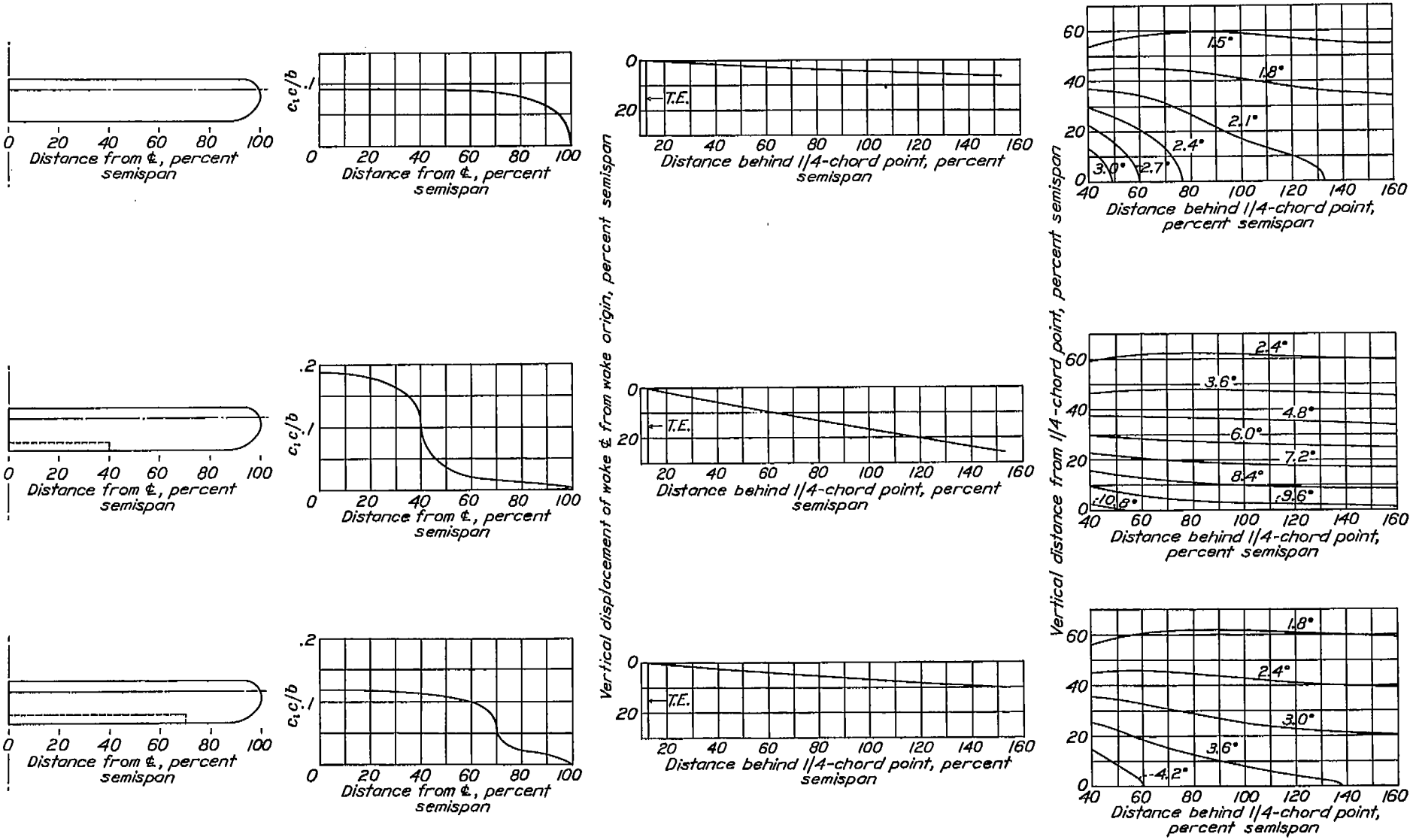

FIGURE 3.—Design charts showing load distribution, downwash displacement, and downwash angles. Plain wing, 0.4b and 0.7b flaps; C_L and C_{l_p} 1.0; taper, 1:1; aspect ratio, 12.

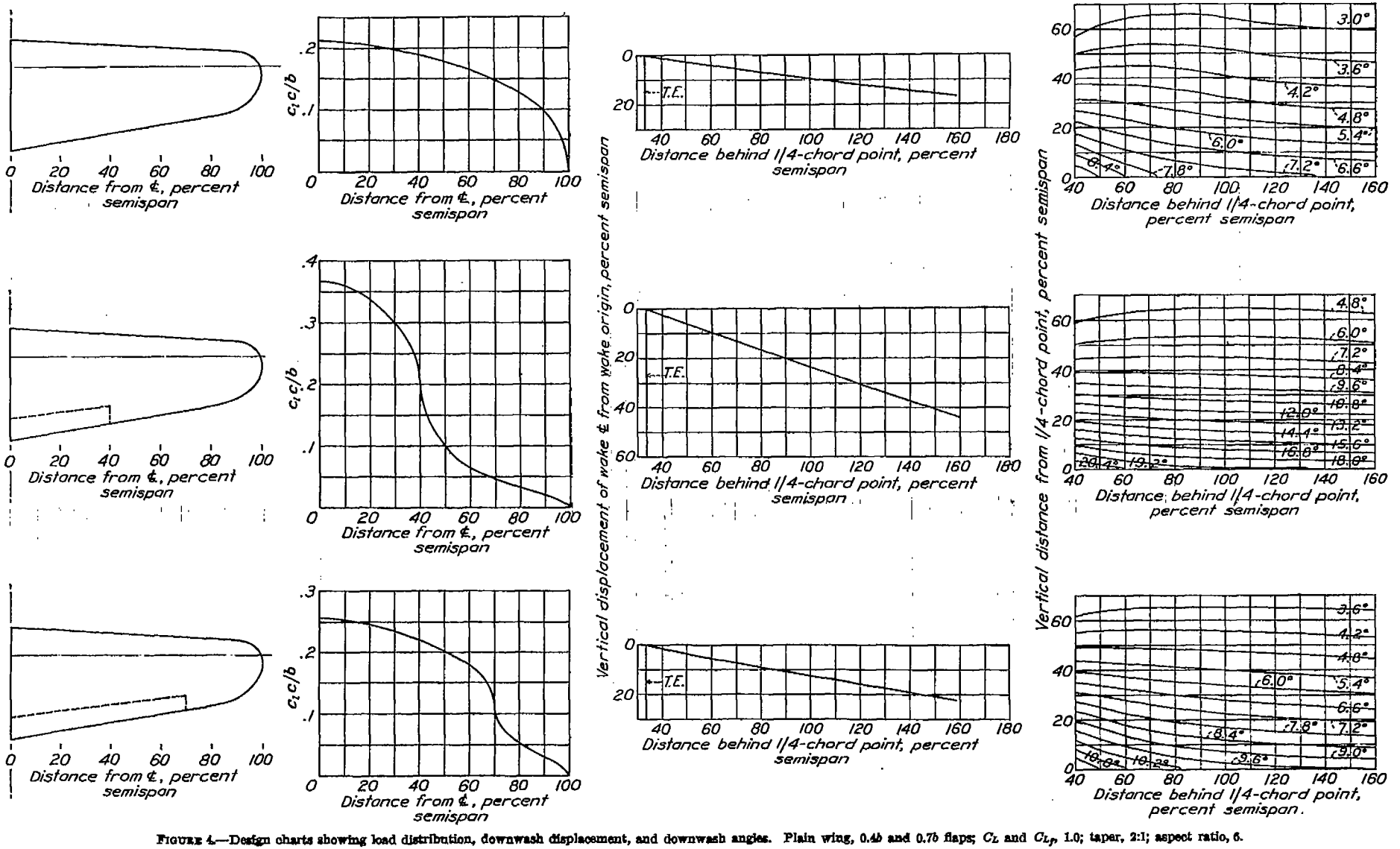

FIGURE 4.—Design charts showing load distribution, downwash displacement, and downwash angles. Plain wing, 0.4b and 0.7b flaps; C_L and C_{L_p} 1.0; taper, 2:1; aspect ratio, 6.

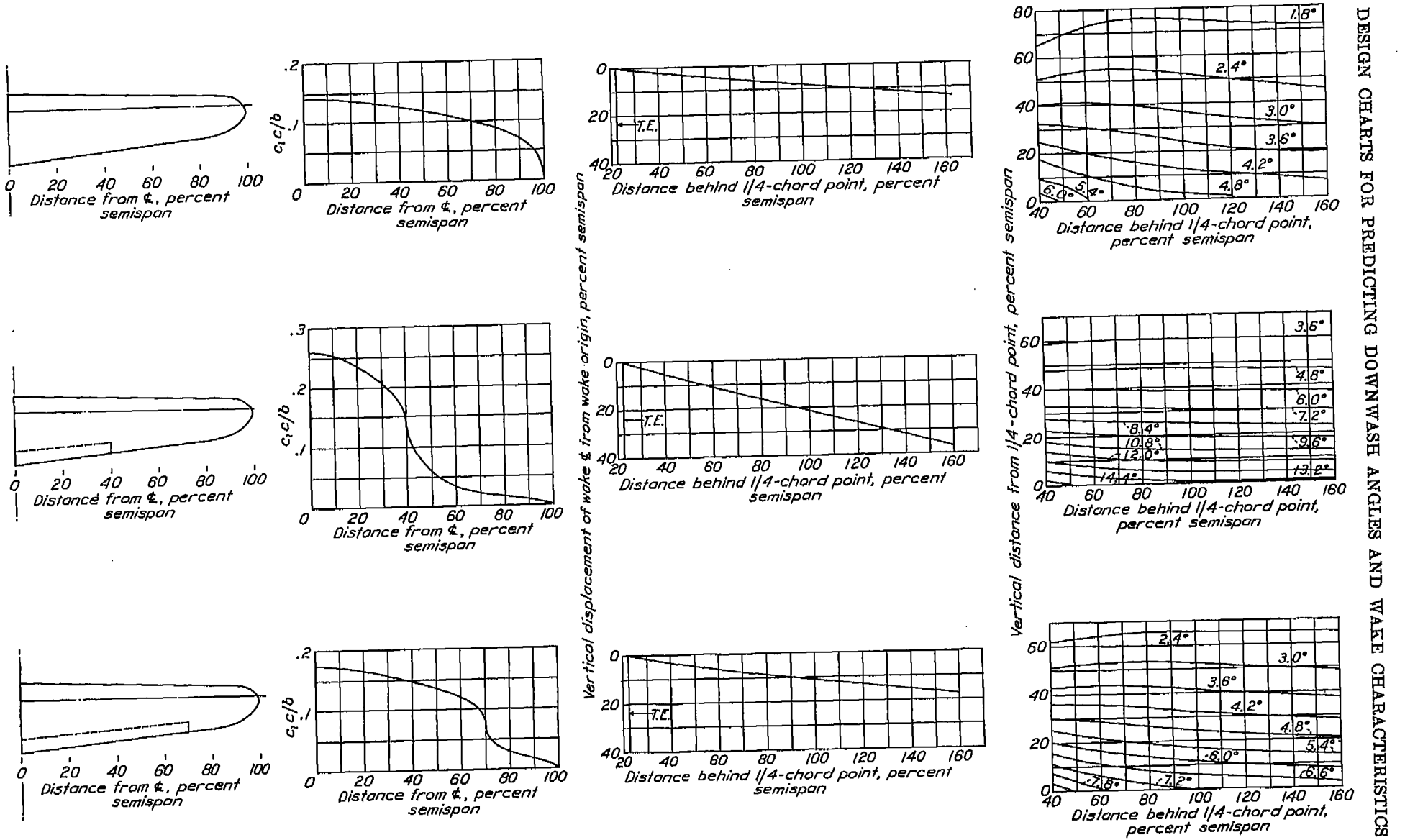

FIGURE 5.—Design charts showing load distribution, downwash displacement, and downwash angles. Plain wing, 0.4b and 0.7b flaps; C_L and C_{L_f}, 1.0; taper, 2:1; aspect ratio, 9.

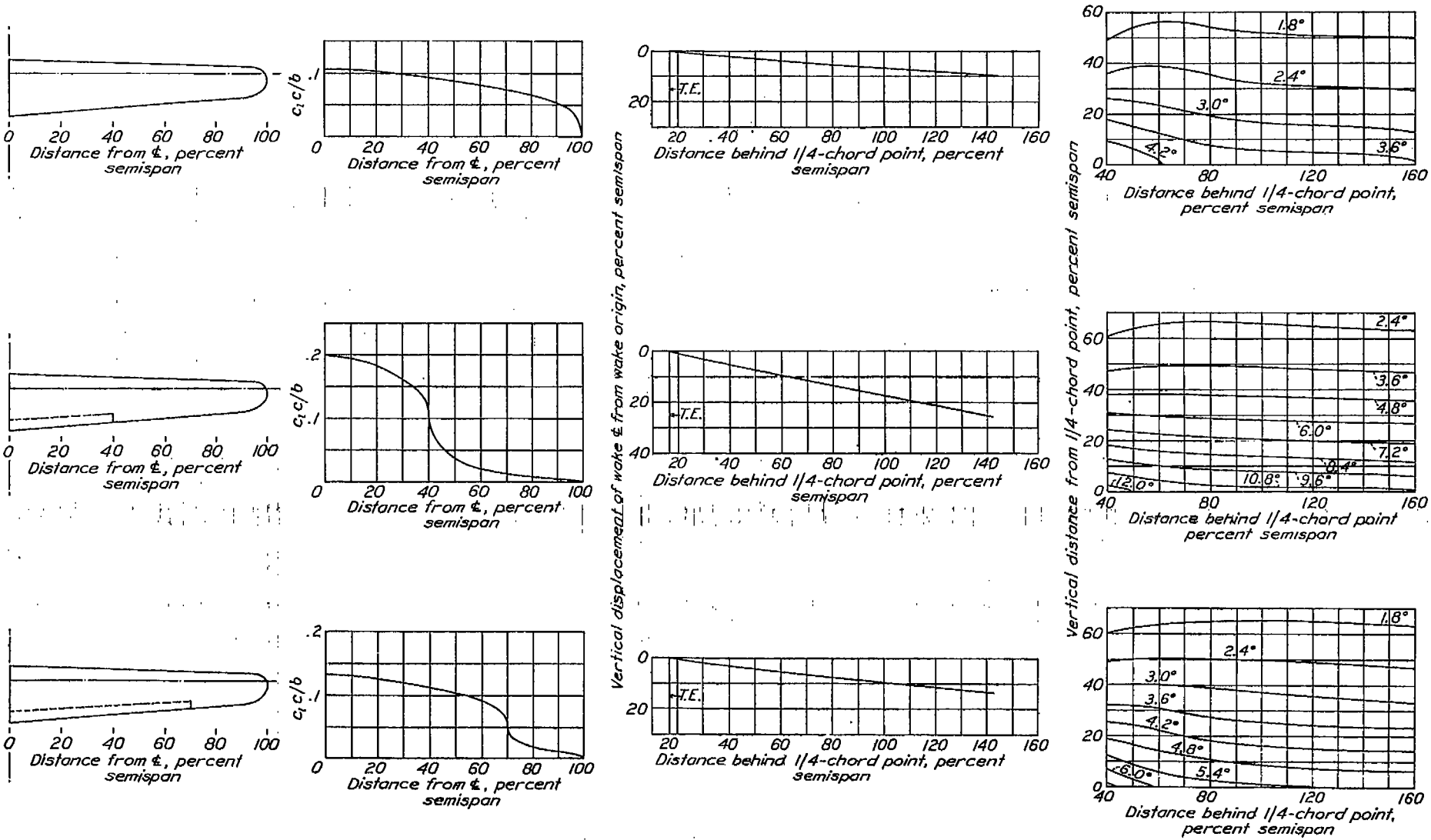

FIGURE 6.—Design charts showing load distribution, downwash displacement, and downwash angles. Plain wing, 0.4b and 0.7b flaps; C_L and C_{L_F} 1.0; taper, 2:1; aspect ratio, 12.

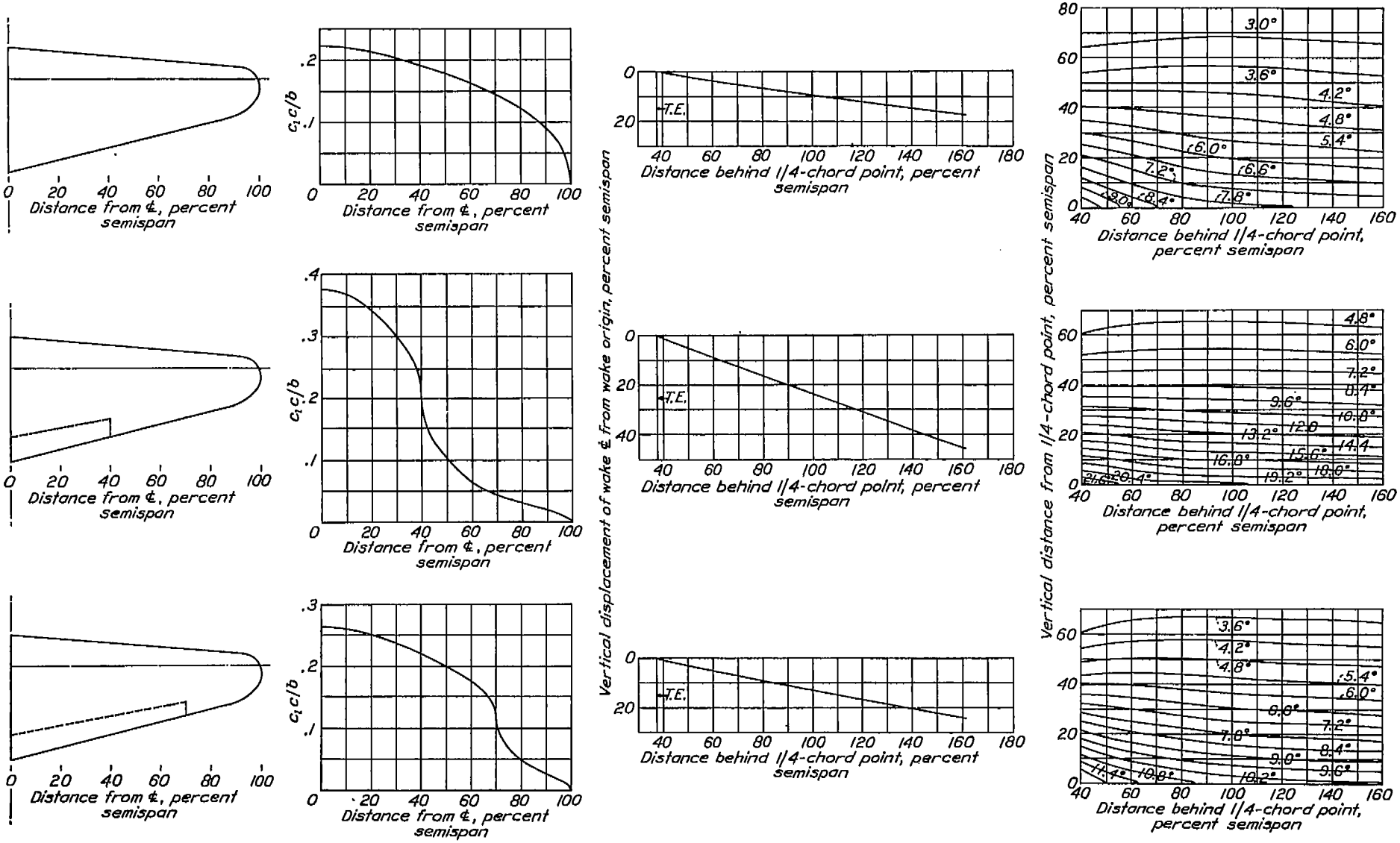

FIGURE 7.—Design charts showing load distribution, downwash displacement, and downwash angles. Plain wing, 0.4b and 0.7b flaps; C_L and C_{l_p}, 1.0; taper, 3:1; aspect ratio, 6.

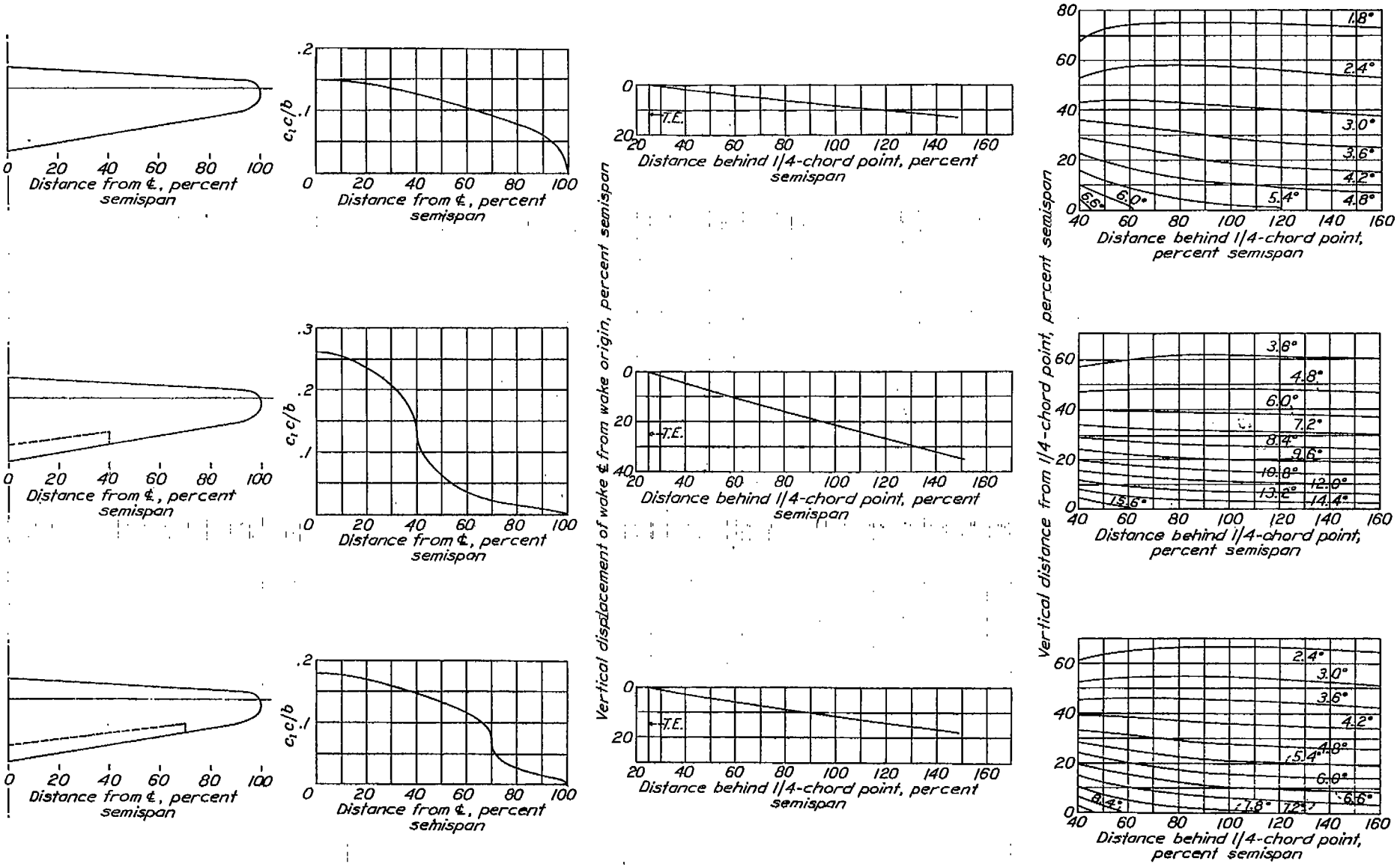

FIGURE 8.—Design charts showing load distribution, downwash displacement, and downwash angles. Plain wing, 0.4b and 0.7b flaps; C_L and C_{L_p} 1.0; taper, 3:1; aspect ratio, 9.

209142—40——9

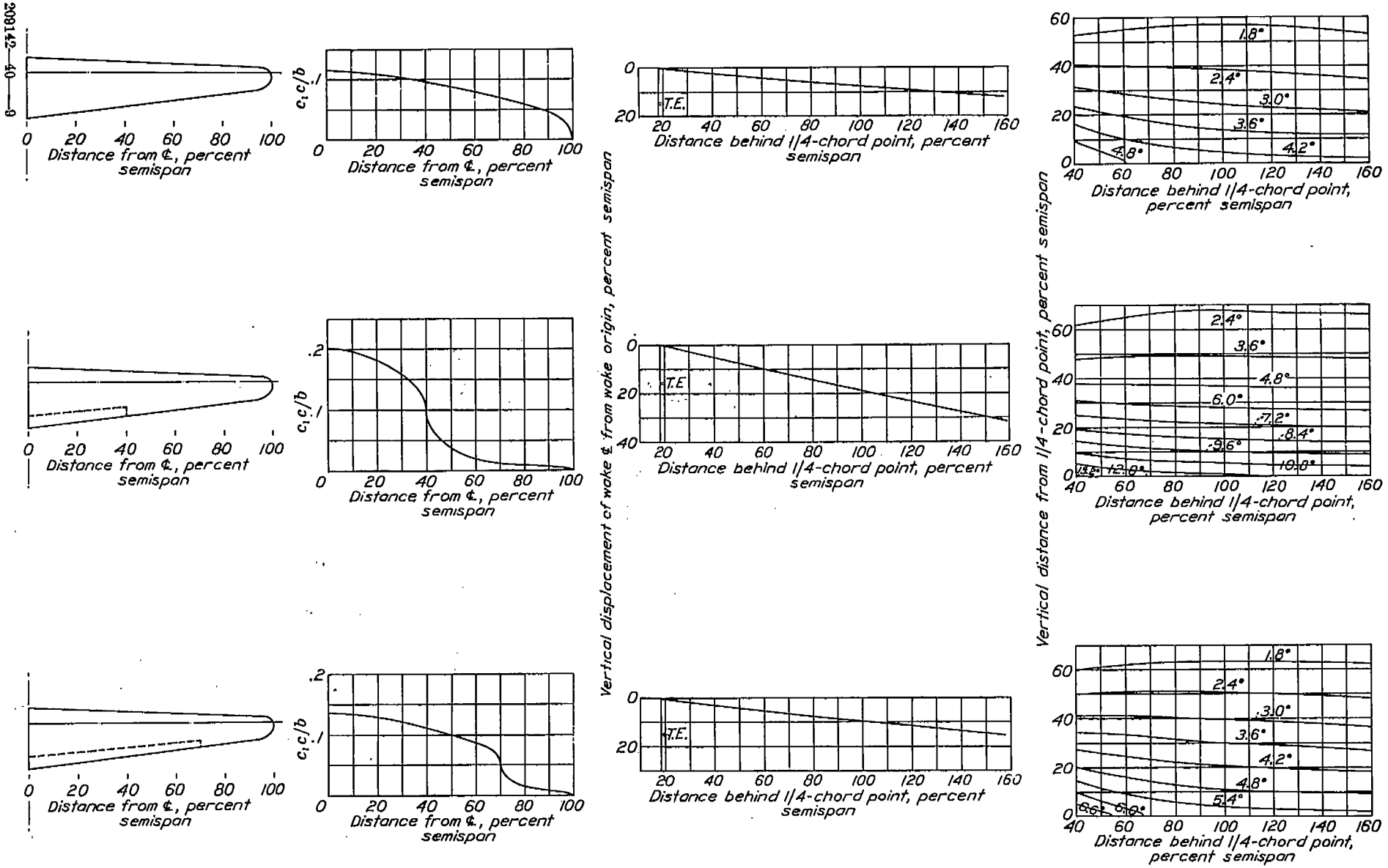

FIGURE 9.—Design charts showing load distribution, downwash displacement, and downwash angles. Plain wing, 0.4b and 0.7b flaps; C_l and C_{L_f}, 1.0; taper, 3.1; aspect ratio, 12

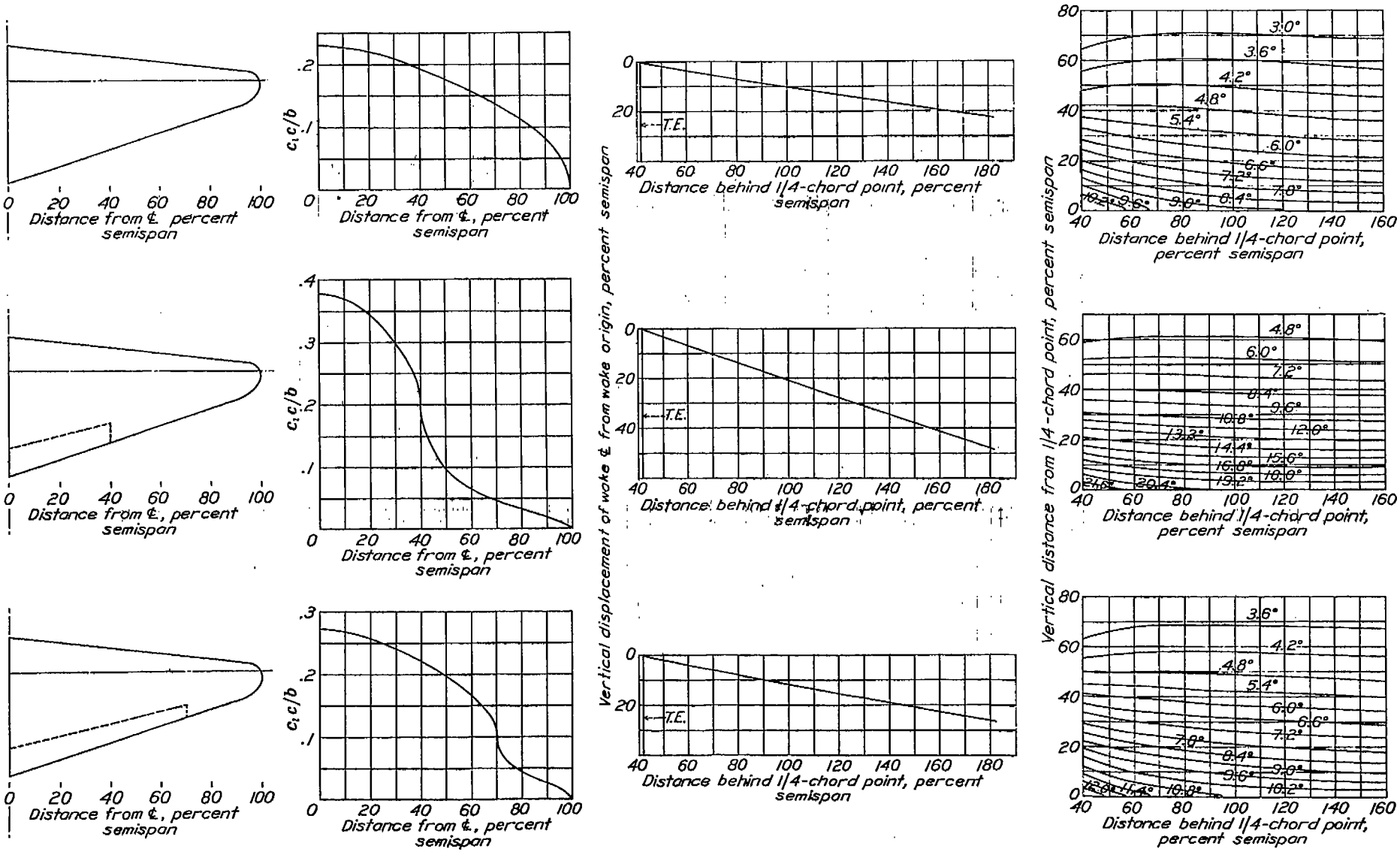

FIGURE 10.—Design charts showing load distribution, downwash displacement, and downwash angles. Plain wing, 0.4*b* and 0.7*b* flaps; C_L and C_{l_c} 1.0; taper, 5:1; aspect ratio, 6.

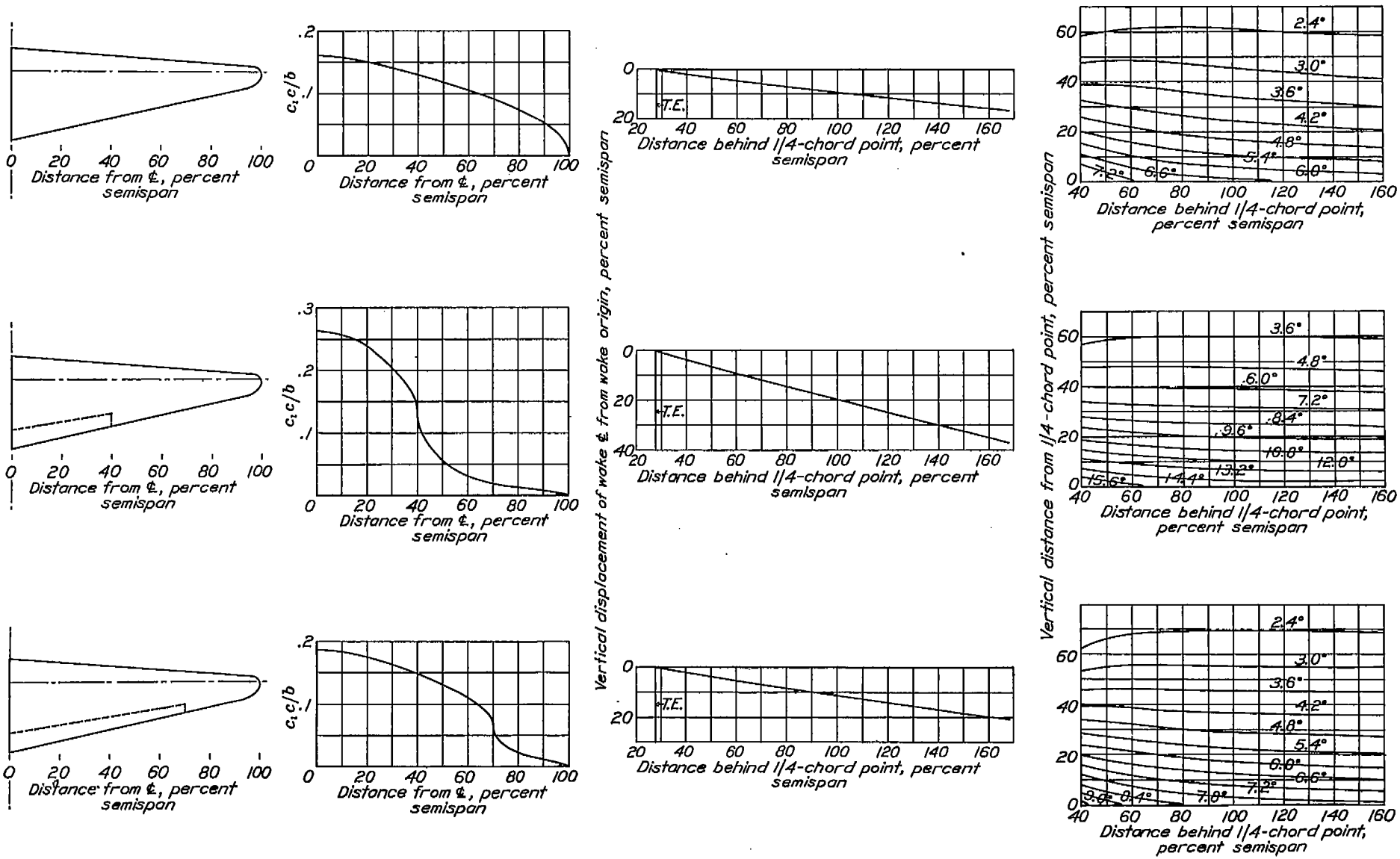

FIGURE 11.—Design charts showing load distribution, downwash displacement, and downwash angles. Plain wing, 0.4b and 0.7b flaps; C_L and C_{L_p}, 1.0; taper, 5:1; aspect ratio 9.

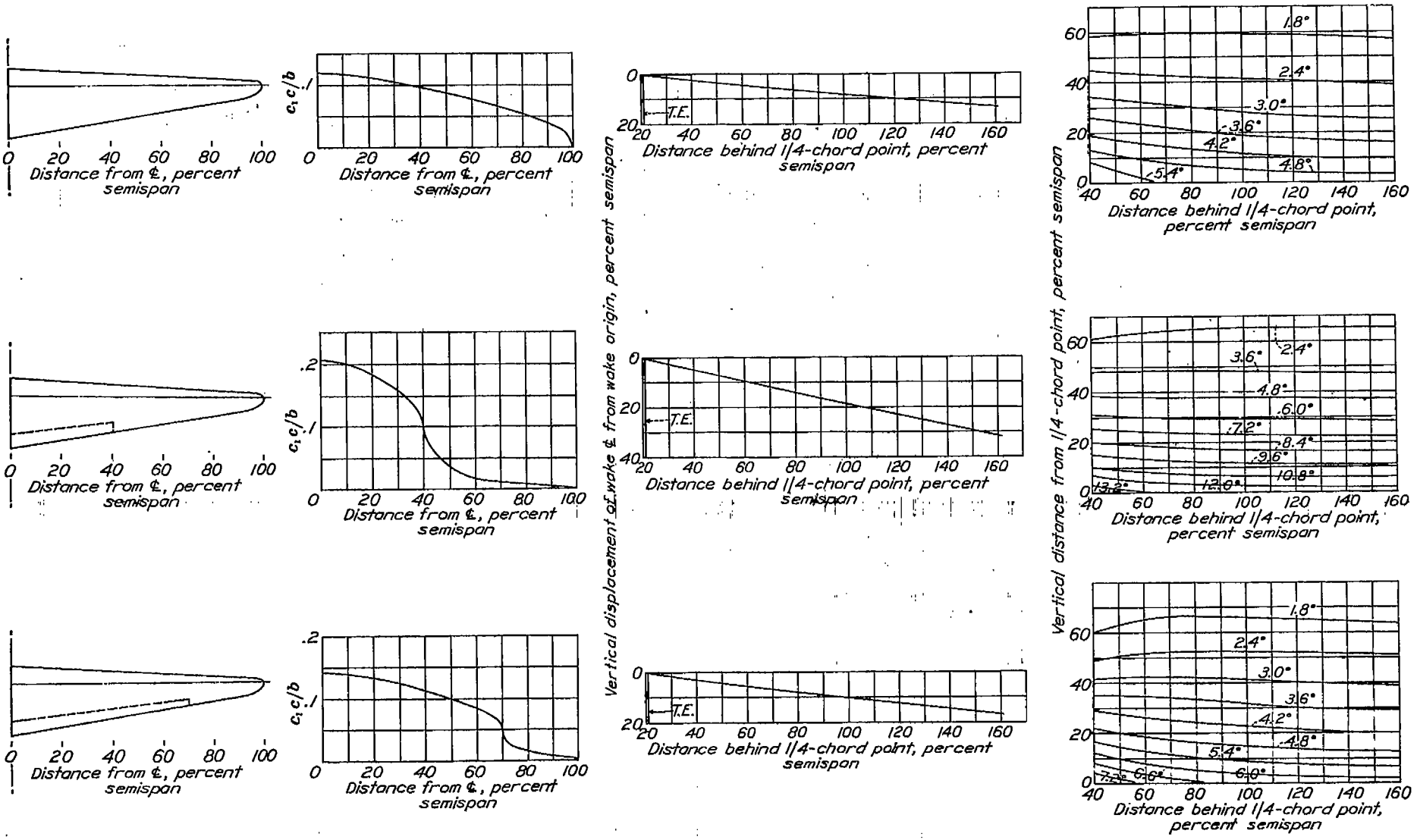

FIGURE 12.—Design charts showing load distribution, downwash displacement, and downwash angles. Plain wing, 0.4b and 0.7b flaps; C_L and C_{L_f}, 1.0; taper, 5:1; aspect ratio, 12.

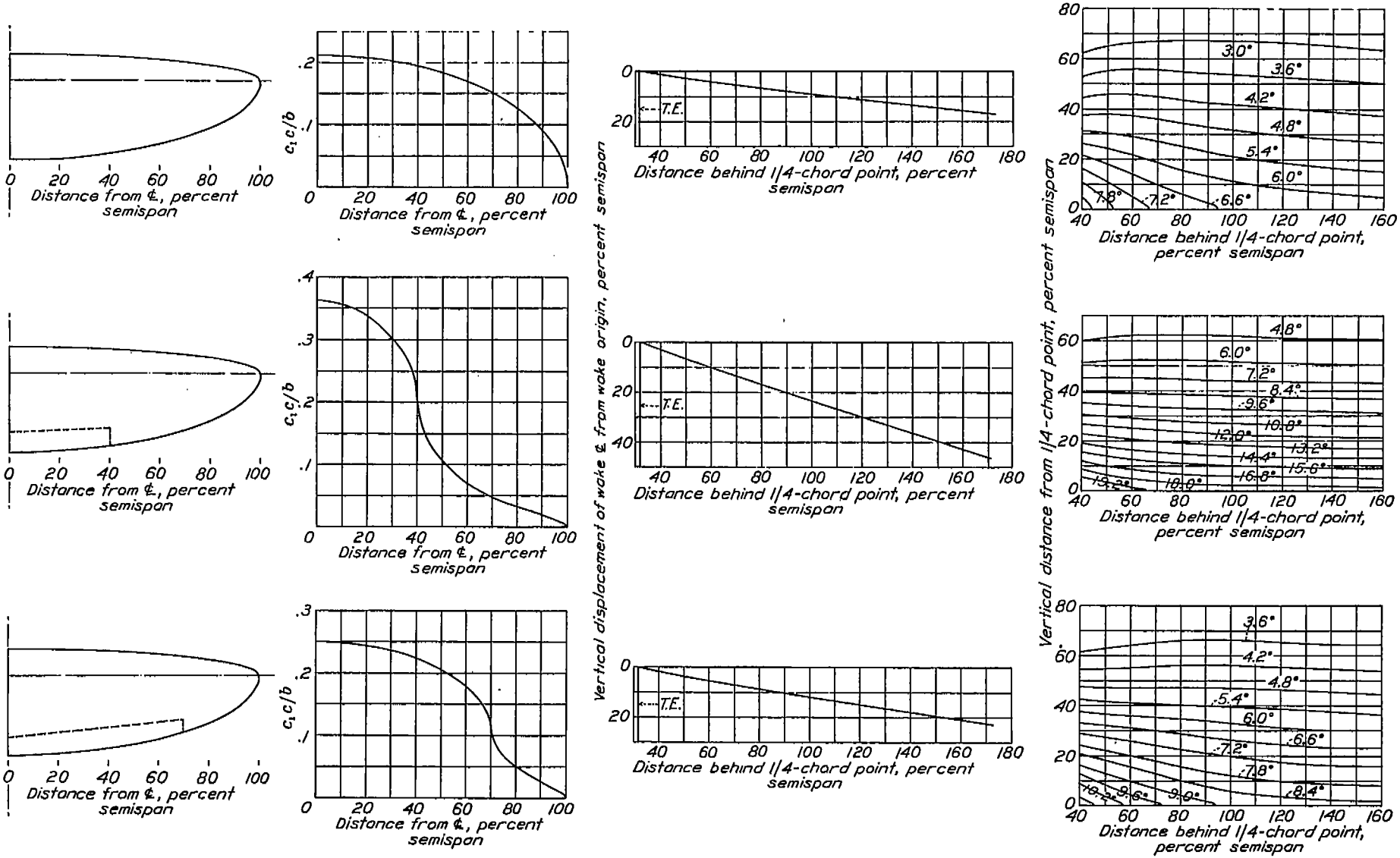

FIGURE 13.—Design charts showing load distribution, downwash displacement, and downwash angles. Plain wing, 0.4b and 0.7b flaps; C_L and C_{l_f}, 1.0; elliptical; aspect ratio, 6.

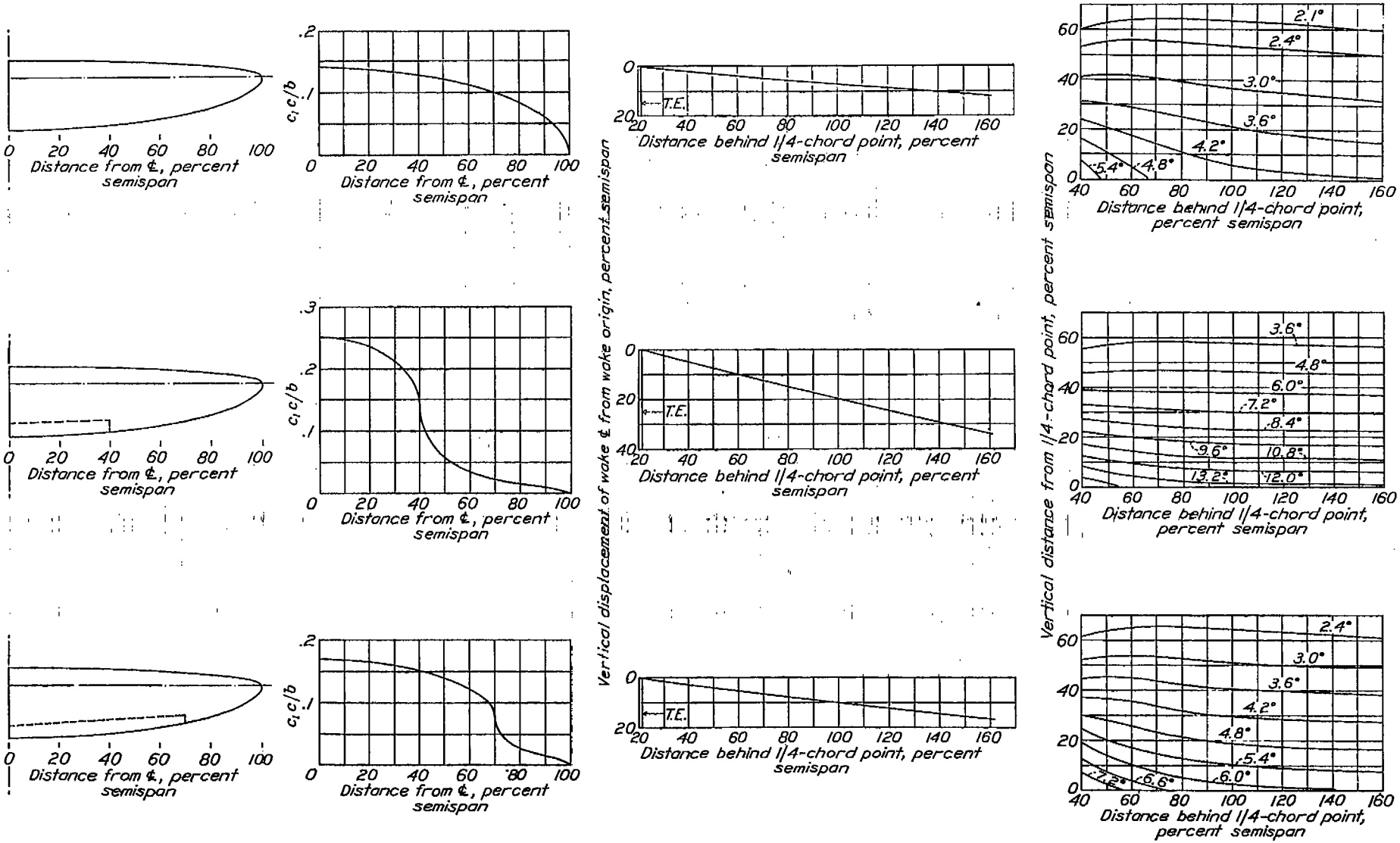

FIGURE 14.—Design charts showing load distribution, downwash displacement, and downwash angles. Plain wing, 0.4b and 0.7b flaps; C_L and C_{L_f}, 1.0; elliptical; aspect ratio, 9.

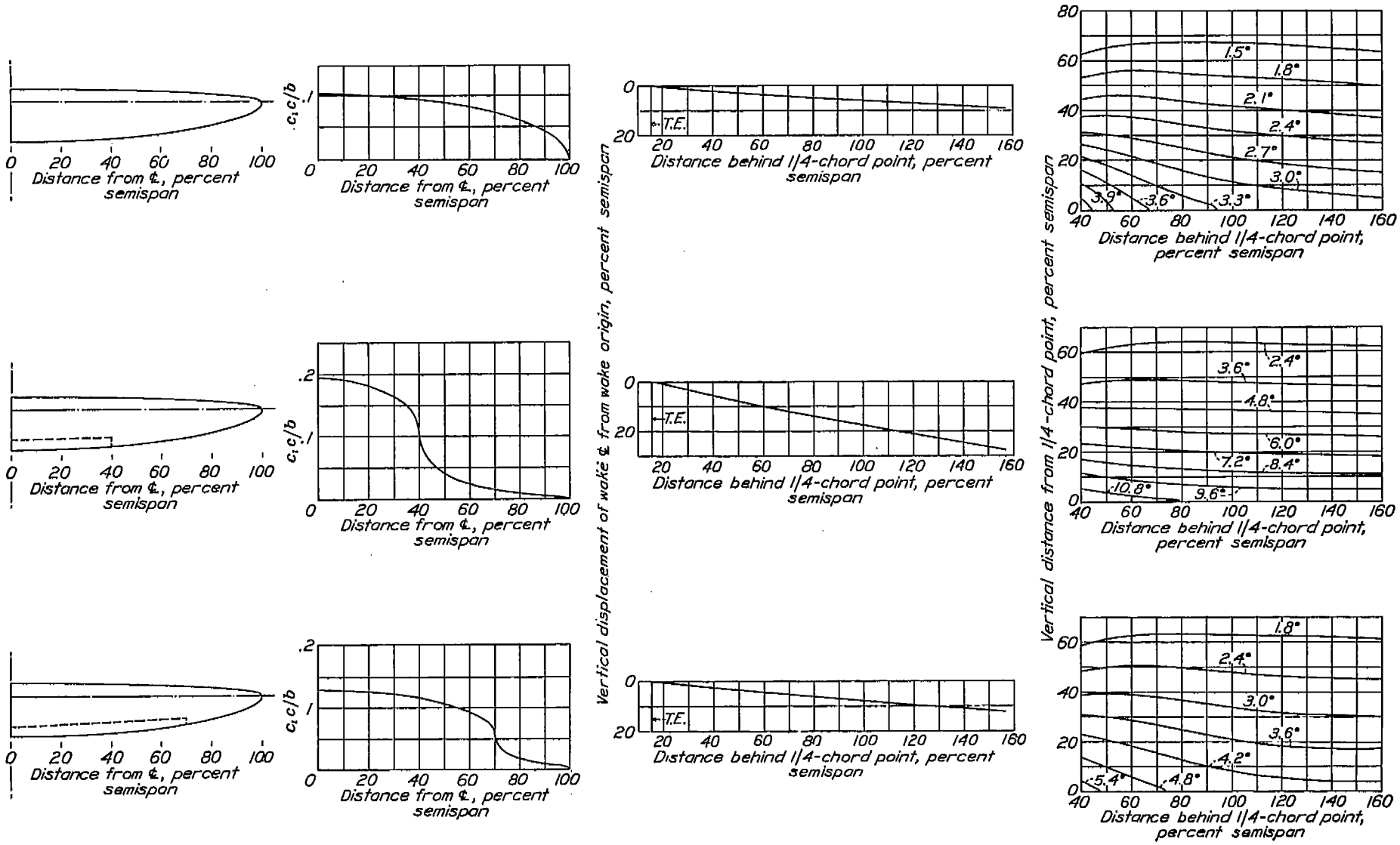

FIGURE 15.—Design charts showing load distribution, downwash displacement, and downwash angles. Plain wing, 0.4b and 0.7b flaps; C_L and C_{L_f}, 1.0; elliptical; aspect ratio, 12.

Undisplaced downwash-contour charts.—The downwash-contour charts shown in the fourth column are drawn for $C_{L_w}=1.0$ and $C_{L_f}=1.0$. For other lift coefficients, the downwash angles can be obtained by multiplying the angles on the contour charts by the particular values of C_{L_w} or C_{L_f}. In the derivation of these charts, the trailing vortex sheet was assumed to start at the quarter-chord line and to extend unchanged indefinitely downstream. As already explained, the vortex system is thereby assumed to be made up of U-vortices of strength $-(d\Gamma/ds)ds$, where Γ is the strength of the bound vortex. The downflow velocity at a point (x, z) in the symmetry plane is given by the equation

$$w=-\frac{1}{\pi b}\int_0^1 s\frac{d\Gamma}{ds}\left[\frac{x}{\sqrt{s^2+x^2+z^2}}\left(\frac{1}{x^2+z^2}+\frac{1}{s^2+z^2}\right)+\frac{1}{s^2+z^2}\right]ds \quad (1)$$

In the actual computation, the indicated integration was replaced by a summation, i. e., the smooth span load distributions were approximated by stepwise distributions of 5 to 7 steps, so that equation (1) was effectively replaced by

$$w=-\frac{1}{\pi b}\sum_1^n s_n(\Delta\Gamma)_n\left[\frac{x}{\sqrt{s_n^2+x^2+z^2}}\left(\frac{1}{x^2+z^2}+\frac{1}{s_n^2+z^2}\right)+\frac{1}{s_n^2+z^2}\right] \quad (2)$$

where $(\Delta\Gamma)_n$ is the rise of the nth step and s_n is the corresponding semispan. Figure 16 illustrates the substitution of a stepwise distribution for a continuous span load distribution.

Curves of the function

$$g=\frac{s}{2\pi}\left[\frac{x}{\sqrt{s^2+x^2+z^2}}\left(\frac{1}{x^2+z^2}+\frac{1}{s^2+z^2}\right)+\frac{1}{s^2+z^2}\right]$$

were found useful in these computations. They are reproduced in figure 17.

The longitudinal component of the induced flow generally being negligible compared with the free-stream velocity V, it follows that the tangent of the downwash angle is very nearly w/V. The downwash-contour charts have been constructed on this basis; only half of each chart is shown, for the axis is a line of symmetry when the longitudinal components of the induced velocities are neglected.

Displacement of the center line.—The downwash-contour charts just described require a vertical displacement, as has already been mentioned, because the trailing vortex sheet undergoes downward displacement as it proceeds downstream. The downward displacement is given by the equation

$$h=\int_{T.E.}^{x}\tan\epsilon\,dx \quad (3)$$

The curves shown in the third column of figures 1 to 15 are plots of this integral as a function of x, for $C_{L_w}=1.0$ and $C_{L_f}=1.0$. For other lift coefficients, displacements are obtained by multiplying the values on the charts by the particular values of C_{L_w} or C_{L_f}.

Origin of the trailing vortex sheet.—For a plain wing, the sheet is considered to be shed at the trailing edge. For a wing with a flap, the origin is between the trailing edges of the flap and the wing,

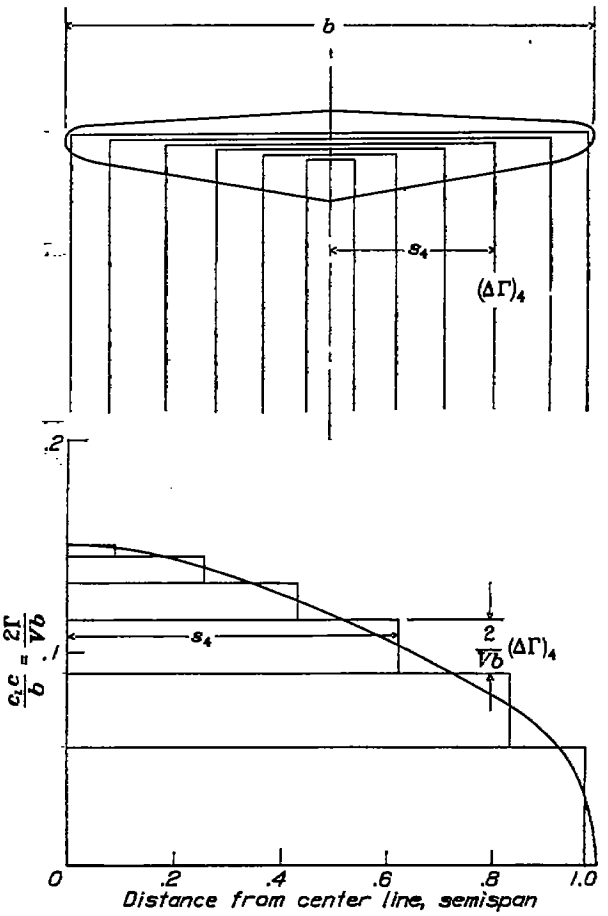

FIGURE 16.—Illustration of the substitution of six U-vortices for the actual vortex system. C_L, 1.0; taper, 3:1; aspect ratio, 9.

the distance below the trailing edge of the wing, in semispans, being given by the formula

$$h_0=\frac{(c_f/2)\sin\delta_f+kc}{b/2} \quad (4)$$

which is based on the available experimental data. The factor k is given in figure 18.

Contribution of the flap to the total lift.—Figure 19 shows the theoretical contribution of the flap to the wing lift coefficient. The values of $C_{L_f}/\Delta c_l$ were derived incidental to the computations of span load distribution, coming directly out of the first term of the Fourier series for the loading. It must be noted that they correspond, as do the span load distributions themselves, to flaps of uniform c_f/c or, stated differently, to flaps of uniform Δc_l. Where Δc_l is not uniform, an average Δc_l weighted according to chord will usually be satisfactory.

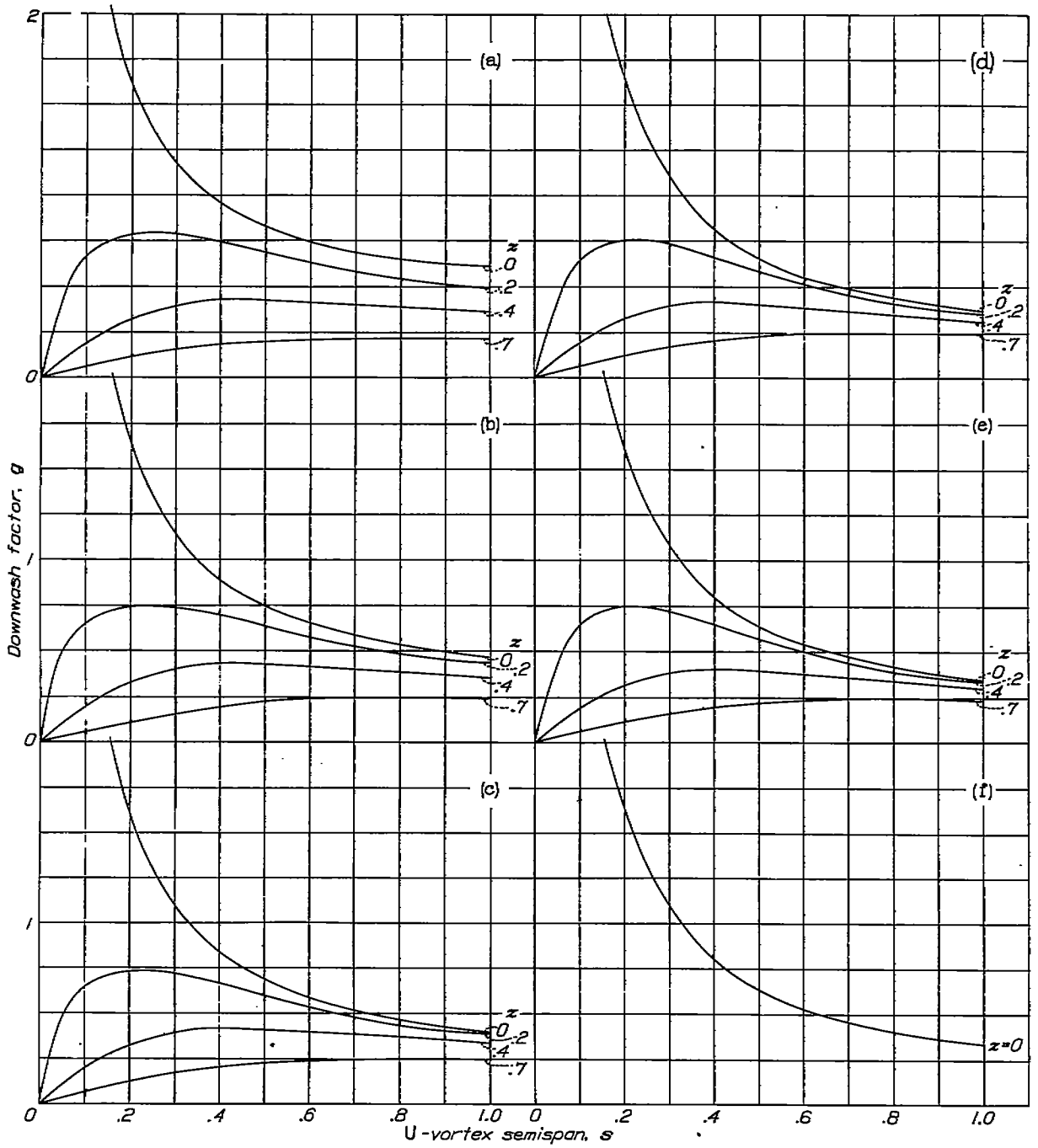

FIGURE 17.—Curves of the g function for various values of x and z. (a) x=0.4. (b) x=0.6. (c) x=0.9. (d) x=1.2. (e) x=1.6. (f) x=2.5.

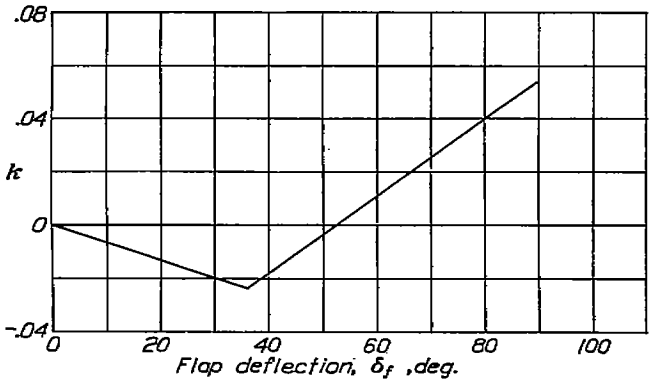

FIGURE 18.—Curve of the k factor for locating the wake origin for wings with flaps.

Curves of Δc_l.—In order to facilitate the application of the curves of figure 19, data are presented in figure 20 for the increment of section lift coefficient Δc_l obtained by deflecting the various flaps. It must be noted that these increments are *section* characteristics and give the increase in lift coefficient when the flap is lowered in two-dimensional flow. The data were obtained mainly from N. A. C. A. results and from reference 5. No attempt has been made here to give a complete presentation of the lift increments due to flaps. The data given are best applicable at about 3° to 4° below maximum lift; however, they apply with reasonable accuracy at lower angles, for the increments are nearly constant

209142—40——10

over the entire useful range. The coefficients for the 0.20c external-airfoil flap are based on the combined chord of the wing and flap; those for the 0.26c Fowler

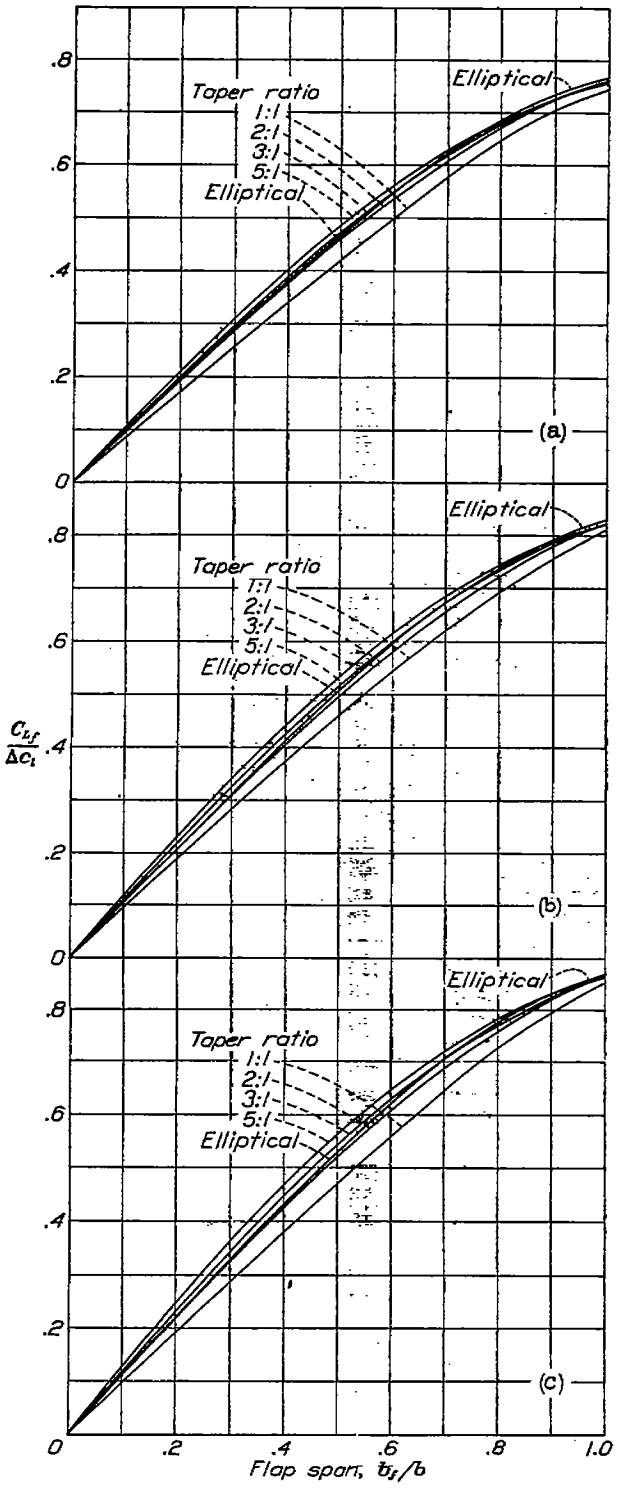

FIGURE 19.—Lift increments for wings with partial-span flaps. (a) $A=6$. (b) $A=9$. (c) $A=12$.

flap are based on the chord of the plain wing. In the case of the Fowler flap, simply extending the flap, with $\delta_f=0°$, increases the lift coefficient by about 26 percent, because the effective chord is increased by this amount. Accordingly, the total increment in lift coefficient on extending the flap is 26 percent of the lift coefficient for the plain wing at the particular angle of attack, plus the further increment given in figure 20 for the particular δ_f.

Variation of downwash across the tail span.—The discussion thus far has been concerned with the calcula-

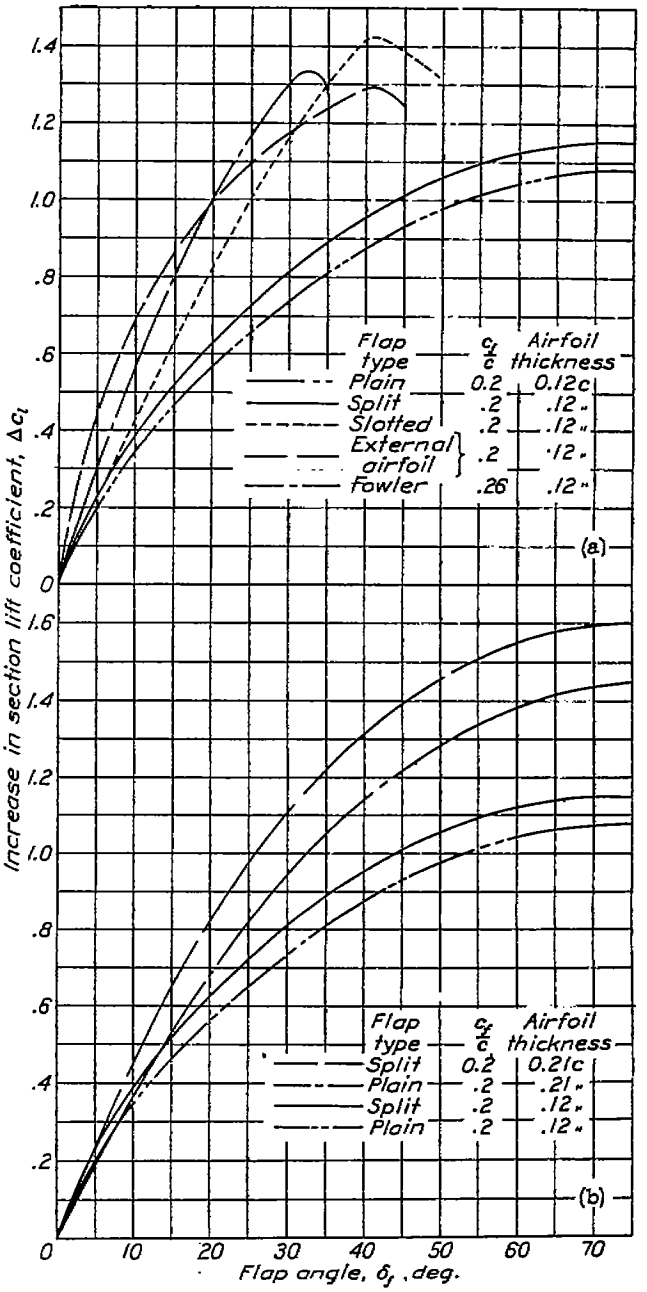

(a) Different types of flap on wings 0.12c thick.
(b) Comparison of flapped wings 0.12c and 0.21c thick.

FIGURE 20.—Increment in section lift coefficient due to flap.

tion of the downwash in the plane of symmetry and it has been tacitly implied that the downwash so derived applies over the entire tail span. In order to investigate the error thereby involved, calculations of downwash were made for points on the vortex sheet, 0.75 $b/2$ back from the quarter-chord line, which is approximately the usual longitudinal position of the tail. The calculations showed that, for some cases, considerable difference exists between the downwash at the center of the tail and the average downwash over the tail.

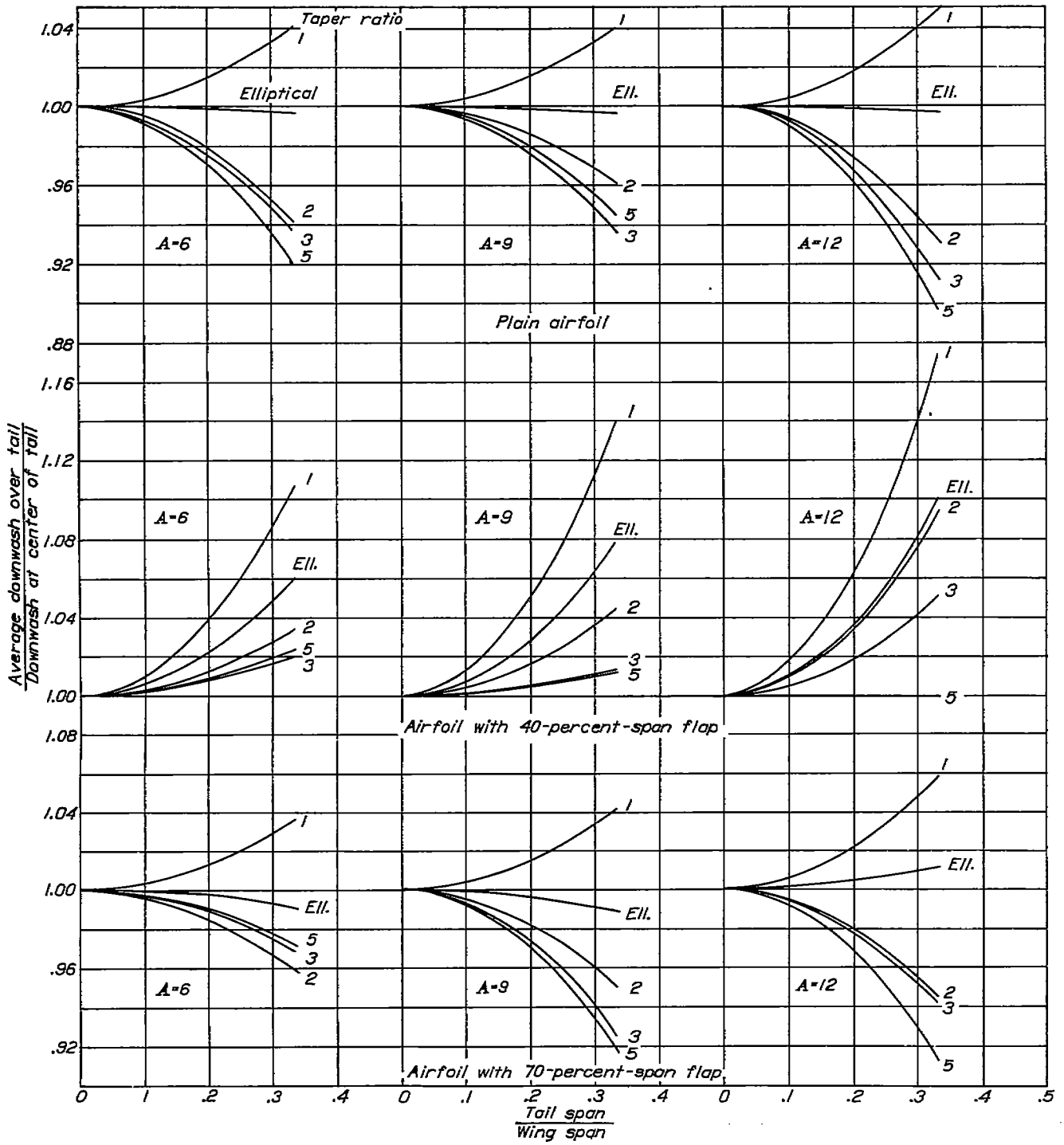

FIGURE 21.—Correction for the variation of downwash across the tail span for $x=0.75\ b/2$.

The correction factors have been plotted in figure 21 for all cases.

METHODS OF APPLICATION

Downwash, plain wings.—The downwash at the tail of an airplane with a wing having neither twist nor a flap is obtained from the charts given in figures 1 to 15 in the following manner:

1. For each angle of attack under consideration, find the longitudinal distance x of the elevator-hinge axis from the quarter-chord point of the root section and the vertical distance m of the hinge axis from the trailing edge, or wake origin. Consider m to be negative if the hinge axis lies below the trailing edge.

2. Find the downward displacement h of the wake center line at distance x from the quarter-chord point by multiplying the value at distance x on the corresponding displacement chart by the lift coefficient C_L.

3. Locate the point $(x, |m+h|)$ on the downwash-contour chart[1] and multiply the corresponding down-

[1] The ordinates of the downwash charts are here applied as "vertical distances from the wake" although, corresponding to the method of derivation of the charts, the ordinate scale is labeled "vertical distance from the ¼-chord point." This interchange is possible because the displacements of the wake center and downwash pattern are equal. (Cf. paragraph 3 of page 2.)

wash angle by the lift coefficient and by the correction factor of figure 21.

Downwash, flapped wings.—For an airplane with flaps down, it is first necessary to separate the lift coefficient into two parts. The part C_{L_w} is the lift coefficient at the particular angle of attack, with flaps up. The part C_{L_f} is the increase, at the particular angle of attack, on lowering the flap; it may be obtained by the use of figures 19 and 20. Derivation of the downwash proceeds in the following manner:

1. Find the longitudinal distance x of the hinge axis from the quarter-chord point of the root section, and the vertical distance m of the hinge axis from the wake origin. The wake origin in this case is not the trailing edge but a point below the trailing edge, as previously explained. (See equation (4).)

2. Find the contribution h_1 of the plain wing to the downward displacement of the wake center line at distance x from the quarter-chord point by multiplying the value on the corresponding displacement chart (plain wing), at distance x, by C_{L_w}.

3. Find the contribution h_2 of the flap to the downward displacement by multiplying the value on the corresponding displacement chart (flap), at distance x, by C_{L_f}.

4. Locate the point $(x, |m+h_1+h_2|)$ on the contour charts for the plain wing and for the flap; multiply the corresponding downwash angles, respectively, by C_{L_w} and C_{L_f} and by the correction factors of figure 21 and add in order to get the desired downwash.

This procedure completes the computation of the downwash, except for the wake effect, which increases the downwash above the wake center line and decreases the downwash below it. The amount of this correction will be discussed in the next section. There are two other reasons, previously mentioned, for making still further corrections, seldom exceeding 0.5°, positive above the wake and negative below it. Interference of the fuselage, the nacelles, and the wing-fuselage junctures is only partly predictable; however, for the modern airplane with efficient wing-fuselage junctures and streamline fuselages, it is likely to be of small importance.

For wings or for flap spans other than those covered by the charts, a linear interpolation is usually permissible. For a wing with appreciable aerodynamic twist, the downwash due to the twist will have to be computed from the span load distribution at $C_L=0$ and applied as an additive correction. Dihedral and sweepback may be neglected.

WAKE CHARTS AND FORMULAS

The center line of the wake coincides with the center line of the trailing vortex sheet; hence no new data are required for locating it. The wake half-width, in chord lengths, is given by the formula

$$\zeta=0.68c_{d_0}^{1/2}(\xi+0.15)^{1/2} \tag{5}$$

in which ξ is in chord lengths. It will be noted that the unit of length in this and the other wake equations is the chord rather than the semispan. Curves of this equation are plotted in figure 22 for different values of the parameter c_{d_0}.

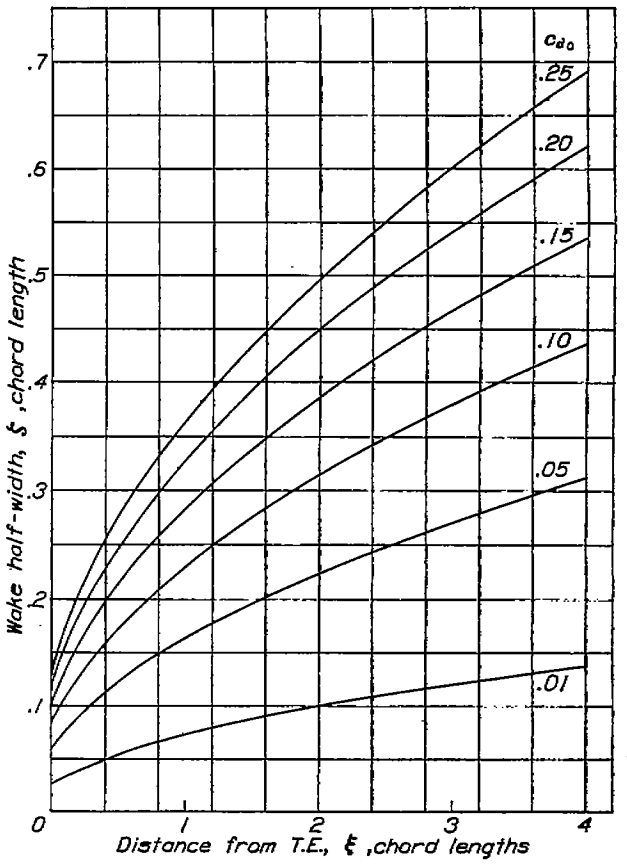

FIGURE 22.—Relation between wake width and distance from trailing edge.
$\zeta=0.68c_{d_0}^{1/2}(\xi+0.15)^{1/2}$

The maximum loss of dynamic pressure in the wake occurs at the wake center and its value η is given by the formula

$$\eta=\frac{2.42c_{d_0}^{1/2}}{\xi+0.3} \tag{6}$$

Curves of this equation are plotted in figure 23 for different values of the parameter c_{d_0}. The distribution of dynamic pressure within the wake is given by the equation

$$\frac{\eta'}{\eta}=\cos^2\left(\frac{\pi}{2}\frac{\zeta'}{\zeta}\right) \tag{7}$$

which is plotted in figure 24.

The effect of the wake on the downwash in and near it is negligible for low profile-drag coefficients as, for example, in the case of plain wings at low angles of attack. It must, however, be taken into account for wings with high-drag flaps and it may be approximately

computed for such cases, as explained in reference 1. Results of some of these computations are shown in figure 25. Figure 25 (a) shows the computed effect at the upper edge of the wake for three distances behind the trailing edge; at the lower edge of the wake, it is the same in magnitude but opposite in sign. The effect diminishes with distance from the wake; for points only a short distance outside the wake (i. e., for the most usual tail positions), however, it is nearly equal to that at the wake edge near it. Figure 25 (b) shows some typical variations of the effect within the wake.

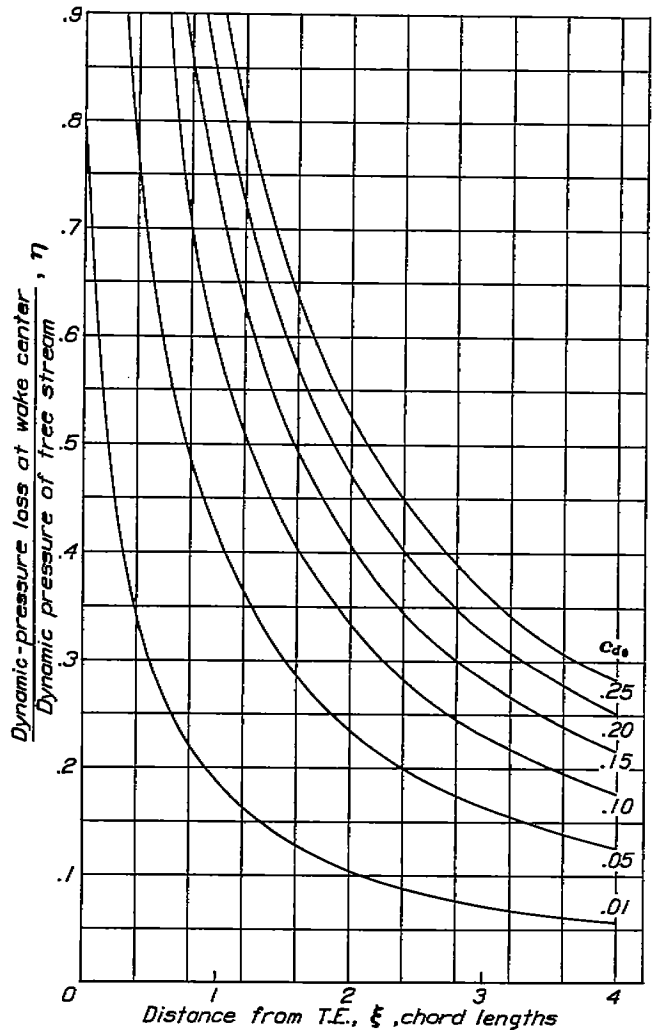

FIGURE 23.—Relation between maximum loss of dynamic pressure in the wake and distance from the trailing edge.

$$\eta = \frac{2.42 c_{d_0}^{1/2}}{\xi + 0.3}$$

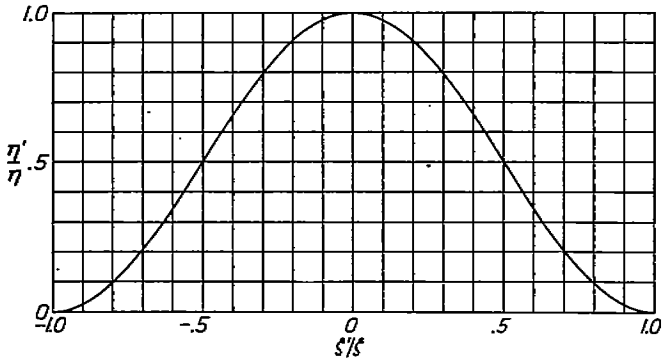

FIGURE 24.—Variation of dynamic-pressure loss across the wake.

$$\frac{\eta'}{\eta} = \cos^2\left(\frac{\pi}{2}\frac{\zeta'}{\zeta}\right)$$

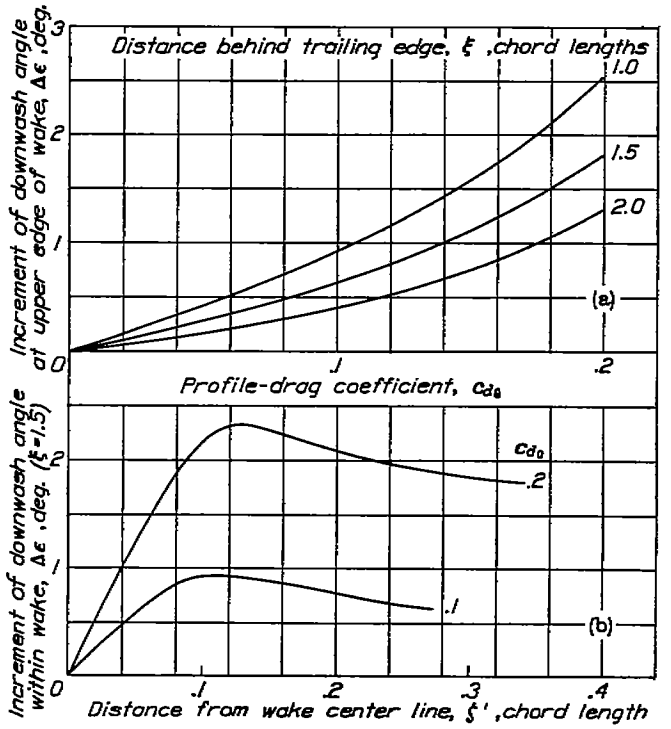

(a) At the upper edge of the wake.
(b) Within the wake.

FIGURE 25.—Wake effect on downwash. The effects are equal, but of opposite sign, below the wake center.

In order to facilitate the application of the preceding equations, which involve c_{d_0}, some section profile-drag coefficients for the different flaps are presented in figure 26. These data apply particularly in the higher lift range, about 3° to 4° below the stall. They were collected mainly from N. A. C. A. results and from reference 5.

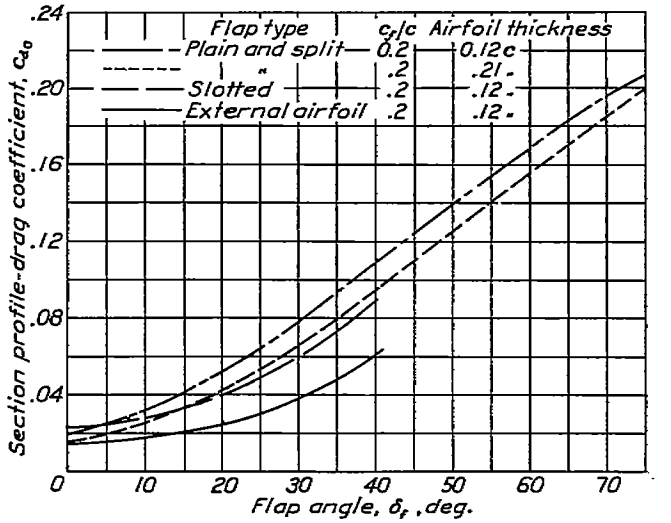

FIGURE 26.—Section profile-drag coefficients for different flaps.

EXAMPLE OF APPLICATION TO DESIGN

For purposes of illustration, some specimen calculations will be made for a midwing monoplane (fig. 27). The wing is of aspect ratio 9, taper ratio 3:1, and has a split flap of 0.70b span and 0.20c chord. This case is covered by figure 8. The tail span is 0.3b.

The case of the airplane with flaps up will be considered first. It will be assumed that, when the airplane is operating at the attitude shown in figure 27 (a),

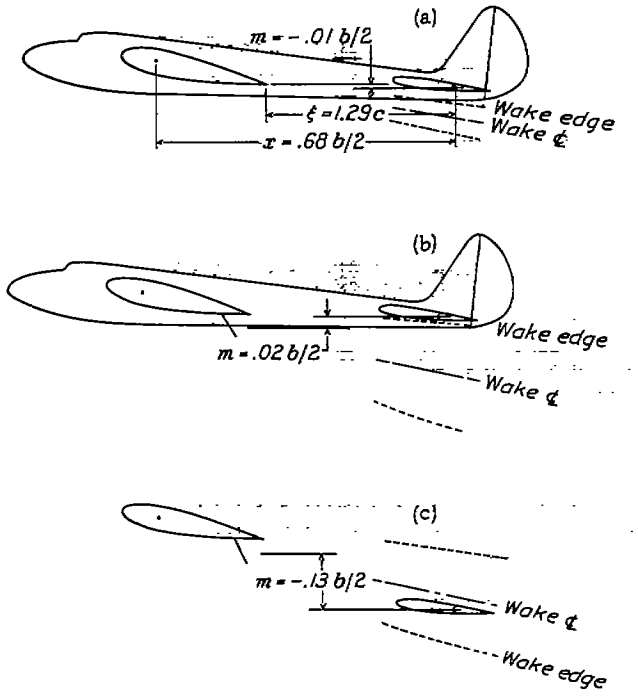

(a) Flap up.
(b) Flap down.
(c) Flap down, tail in the wake.

FIGURE 27.—Illustration for the specimen calculations of downwash and wake.

the lift coefficient C_L is 0.9. The steps outlined under Methods of Application are as follows:

1. $x=0.68\ b/2$. $m=-0.01\ b/2$.

2. The downward displacement of the trailing vortex sheet at $x=0.68\ b/2$ is, for $C_L=1.0$, $0.05\ b/2$, so that $h=0.9\times0.05=0.045\ b/2$.

3. Reference to the downwash-contour chart shows that the downwash at point $(x, |m+h|)$, or (0.68, 0.04), for $C_L=1.0$ is 5.6°. Multiplying by C_L (0.9) and by the correction factor of figure 21 (0.95) gives, for the downwash,

$$\epsilon=0.9\times0.95\times5.6=4.8°$$

The center of the wake passes $m+h$ semispans below the hinge axis, as shown, and its half-width ζ at this point is obtained from the section profile-drag coefficient (assume $c_{d_0}=0.015$) and the distance behind the trailing edge ($\xi=1.29c$), where c may be taken as the root chord. By equation (5) or figure 22,

$$\zeta=0.68\times0.015^{1/2}\times1.44^{1/2}=0.1 \text{ chord}$$

The edges of the wake are shown in the figure. The tail lies outside the wake and, inasmuch as the wake is too slight to affect the downwash, it requires no further consideration.

The airplane at the same attitude, with flap down, $\delta_f=60°$, is shown in figure 27(b). From figure 20, Δc_l is seen to be 1.13 (assuming the wing thickness to be 0.12c); from figure 19, $C_{L_f}/\Delta c_l$ is 0.67, so that $C_{L_f}=0.76$. The contribution of the plain wing, C_{L_w}, is 0.9 as before, since the angle of attack is the same. The steps outlined in Methods of Application are as follows:

1. $x=0.68\ b/2$, as before.
   $m=0.023\ b/2$.
   (The wake origin, as indicated by equation (4) and figure 18, is $\frac{(0.1c)\sin 60°+0.01c}{b/2}$ semispans below the wing trailing edge, at the location shown. For this wing, $b/2=3c$.)
2. The contribution h_1 of the plain wing to the downward displacement is the same as before: $h_1=0.045\ b/2$.
3. For the flap contribution, the chart shows that, for $C_{L_f}=1.0$ and $x=0.68\ b/2$, the displacement is $0.07\ b/2$.
   $h_2=0.76\times0.07=0.053\ b/2$.
4. The point $(x, |m+h_1+h_2|)$ is thus (0.68, 0.12). Reference to the downwash-contour chart for the plain wing and to figure 21 shows that the plain-wing contribution to the downwash at this point is $\epsilon_1=0.9\times0.95\times5.0=4.3°$. Similarly, the flap contribution to the downwash at this point is $\epsilon_2=0.76\times0.94\times6.8=4.9°$. The sum is $\epsilon_1+\epsilon_2=4.3+4.9=9.2°$, to which a wake correction should be applied, as derived in the next paragraph.

The center of the wake in this case passes $m+h_1+h_2=0.12\ b/2$ or 0.36c below the hinge axis, as shown. Figure 26 gives $c_{d_0}=0.17$ and, with $\xi=1.29c$ as before, figure 22 or equation (5) gives the wake half-width:

$$\zeta=0.68\times0.17^{1/2}\times1.44^{1/2}=0.34c$$

The edges of the wake are shown in the figure. There is no effect on the dynamic pressure at the tail, for it lies outside the wake. The increase in downwash at the upper edge is found from figure 25 to be 1.5°. The effect at the tail, which is only a small distance from the edge, may be considered to be the same. The downwash is thus 9.2+1.5=10.7°.

If the relative positions of the wing and tail are such that the tail lies within the wake, as is shown for example in figure 27 (c), the average loss of dynamic pressure at the tail is also required. The loss at the hinge axis may be used for this value although the average over the tail surface may be somewhat different.

The computation of the downwash proceeds as before:

$$x=0.68\ b/2$$

$$m=-0.13\ b/2$$

$$h_1=0.045\ b/2$$

$$h_2=0.053\ b/2$$

$$|m+h_1+h_2|=0.03\ b/2=0.09c$$

$$\epsilon_1=0.9\times0.95\times5.7=4.9°$$

$$\epsilon_2=0.94\times0.76\times7.8=5.6°$$

$\epsilon_1+\epsilon_2=10.5°$, which is the downwash uncorrected for wake effect.

The wake effect at the hinge axis is seen, by interpolating between the two curves of figure 25(b), to be about 1.6°, which must now be *subtracted* from the preceding value, for the tail lies below the wake center. The corrected downwash is $10.5-1.6=8.9°$.

The computation of the dynamic pressure at this point is as follows:

$$\xi=1.29c$$

$$c_{d_0}=0.17$$

$$\zeta=0.34c$$

$$\zeta'=0.09c,\ \frac{\zeta'}{\zeta}=0.26$$

$$\eta=\frac{2.42\times0.17^{\frac{1}{2}}}{1.29+0.3}=0.63,$$ from figure 23 or equation (6).

$$\eta'=0.63\cos^2\left(0.26\frac{\pi}{2}\right)=0.53,$$ from figure 24 or equation (7).

The dynamic pressure at this point is $1-\eta'$, or $0.47q$.

LANGLEY MEMORIAL AERONAUTICAL LABORATORY,
NATIONAL ADVISORY COMMITTEE FOR AERONAUTICS,
LANGLEY FIELD, VA., *July 14, 1938.*

REFERENCES

1. Silverstein, Abe, Katzoff, S., and Bullivant, W. Kenneth: Downwash and Wake Behind Plain and Flapped Airfoils. T. R. No. 651, N. A. C. A., 1939.
2. Anderson, Raymond F.: Determination of the Characteristics of Tapered Wings. T. R. No. 572, N. A. C. A., 1936.
3. Lotz, Irmgard: Berechnung der Auftriebsverteilung beliebig geformter Flügel. Z. F. M., 22. Jahrg., 7. Heft, 14. April 1931, S. 189–195.
4. Pearson, H. A.: Span Load Distribution for Tapered Wings with Partial-Span Flaps. T. R. No. 585, N. A. C. A., 1937.
5. Clark, K. W., and Kirkby, F. W.: Wind Tunnel Tests of the Characteristics of Wing Flaps and Their Wakes. R. & M. No. 1698, British A. R. C., 1936.